

Poisoning the Pixels: Revisiting Backdoor Attacks on Semantic Segmentation

Guangsheng Zhang¹ Huan Tian¹ Leo Zhang² Tianqing Zhu³
Ming Ding⁴ Wanlei Zhou³ Bo Liu¹

¹University of Technology Sydney ²Griffith University
³City University of Macau ⁴Data61, CSIRO, Australia

Abstract

Semantic segmentation models are widely deployed in safety-critical applications such as autonomous driving, yet their vulnerability to backdoor attacks remains largely under-explored. Prior segmentation backdoor studies transfer threat settings from existing image classification tasks, focusing primarily on object-to-background mis-segmentation. In this work, we revisit the threats by systematically examining backdoor attacks tailored to semantic segmentation. We identify four coarse-grained attack vectors (Object-to-Object, Object-to-Background, Background-to-Object, and Background-to-Background attacks), as well as two fine-grained vectors (Instance-Level and Conditional attacks). To formalize these attacks, we introduce BADSEG, a unified framework that optimizes trigger designs and applies label manipulation strategies to maximize attack performance while preserving victim model utility. Extensive experiments across diverse segmentation architectures on benchmark datasets demonstrate that BADSEG achieves high attack effectiveness with minimal impact on clean samples. We further evaluate six representative defenses and find that they fail to reliably mitigate our attacks, revealing critical gaps in current defenses. Finally, we demonstrate that these vulnerabilities persist in recent emerging architectures, including transformer-based networks and the Segment Anything Model (SAM), thereby compromising their security. Our work reveals previously overlooked security vulnerabilities in semantic segmentation, and motivates the development of defenses tailored to segmentation-specific threat models.

1 Introduction

Semantic segmentation is a fundamental computer vision task that assigns a class label to every pixel in an image [35, 41, 54]. It enables pixel-level scene understanding for safety-critical applications such as autonomous driving [14, 17, 45], medical imaging [1, 53], and remote sensing [49]. Despite their widespread deployment, segmentation models remain

vulnerable to malicious security threats, such as backdoor attacks [18].

Backdoor attacks implant hidden triggers during training, typically via data poisoning. A backdoored model behaves normally on clean inputs but produces targeted outputs once the trigger appears at test time. They have been extensively studied in classification tasks [18, 25, 29, 37, 61] as the attacks can lead to catastrophic consequences in safety-critical applications. For example, autonomous driving is built on perception models that reliably identify roads, pedestrians, vehicles, and obstacles. Once triggered, a backdoor can cause the misidentification of obstacles or pedestrians, leading to severe accidents. These risks motivate the examination of backdoor threats in perception models. In this work, we investigate the threats in semantic segmentation.

Existing segmentation backdoor attacks are adapted from image classification. They focus on injecting a trigger into the image to misclassify target objects as background. Differently, they propose distinct trigger designs. For example, HBA [28] adopts a static black line as a global trigger, whereas OFBA [40] embeds high-contrast patches directly on target objects. In contrast, IBA [23] places image patches, such as “Hello Kitty” logos, near the objects to induce background misclassification.

Limitations Despite these initial explorations, existing studies exhibit common limitations: **L1**, they focus on a single attack vector: “object-to-background” attacks. This leaves other vectors in segmentation unexamined, such as “object-to-object” and “background-to-object”. These unexplored vectors can also pose severe security threats and lead to catastrophic consequences. **L2**, existing studies build on trigger designs adapted from image classification. These heuristic designs, however, do not reliably deliver strong attack performance in semantic segmentation. Achieving high attack efficacy requires strategies tailored to segmentation. **L3**, existing studies mainly target conventional CNN-based models. Yet, the vulnerabilities of recent architectures, such as Transformers or the Segment Anything Model (SAM), remain unexplored.

Table 1: Comparison of segmentation backdoor attacks.

Method	Attack Vectors	Trigger Design	Label Manipulation	Attack Stealthiness
HBA [28]	Single	Heuristic	Fixed	Limited
OFBA [40]	Single	Heuristic	Fixed	Limited
IBA [23]	Single	Heuristic	Fixed	Limited
Ours	Multiple	Optimized	Optimized	Enhanced

Research Questions To address these limitations, we formulate the following research questions:

- **RQ1:** Are existing segmentation backdoor settings sufficient to capture real threats? Can we identify other threats beyond the objects-to-background mis-segmentation?
- **RQ2:** Are existing trigger designs sufficient for reliable segmentation backdoor attacks? Can we develop segmentation-aware strategies for more effective attacks?
- **RQ3:** Are the emerging architectures, such as Vision Transformers or Segment Anything Model (SAM), also vulnerable to these attacks? Can we devise effective attacks against these architectures?

Guided by these questions, we present an in-depth study of backdoor attacks in semantic segmentation. We select autonomous driving as our primary application scenario, as it is safety-critical and widely deployed.

Our Approach We structure our investigation as follows to explore answers (A1–A3) to RQ1–RQ3:

A1. Revisited attacks threats: To address RQ1, we reexamine the attack vector for semantic segmentation. We identify multiple overlooked vulnerabilities and organize them into two categories: coarse-grained attacks defined by semantic impact and fine-grained attacks defined by activation conditions.

- **Coarse-grained attacks:** (1) *Object-to-Object Attack* mis-segments an object as a different object class, causing incorrect object perception. (2) *Object-to-Background Attack* erases objects by relabeling them as background, inducing object disappearance. (3) *Background-to-Object Attack* fabricates objects by turning background regions into foreground objects, leading to false positives. (4) *Background-to-Background Attack* mislabels stuff regions such as road and sky, disrupting scene understanding.
- **Fine-grained attacks:** (1) *Instance-Level Attack* targets selective object instances within an image rather than all instances. (2) *Conditional Attack* activates under specific contextual or environmental conditions, enhancing attack stealthiness.

Compared to prior studies, we conduct a more detailed analysis of segmentation backdoor threats. Table 1 summarizes the differences.

A2. Optimized attack framework: To address RQ2, we develop a unified framework, BADSEG (BAckDoor attacks on semantic SEGmentation), for efficient attacks. BADSEG aims to determine effective trigger parameters and victim–target label pairs. For trigger parameters, we reformulate it as an

end-to-end optimization problem. Directly optimizing these parameters is challenging, as many of them are discrete. To overcome this, we leverage the Gumbel-Softmax relaxation [20, 39], which enables differentiable search over the discrete trigger space.

For label manipulation, we select effective victim–target pairs by measuring their semantic distance. Inspired by prior studies [19, 56, 58], we compute inter-class semantic distances and select pairs with minimal distances. By targeting these pairs, we exploit their feature similarity to ensure more efficient attacks. Moreover, to evaluate the proposed attacks, we benchmark them against six representative backdoor defenses. Our results show that these defenses provide limited protection and fail to reliably mitigate the proposed attacks.

A3. Validated attacks on emerging architectures: To address RQ3, we validate BADSEG on the recent segmentation architectures of Transformers and SAM. For Transformers, our results confirm that BADSEG generalizes effectively across all attack vectors.

For SAM, we adapt our attacks because, unlike conventional segmentation models, SAM predicts prompt-conditioned binary masks without explicit class labels. We therefore introduce BADSEG-SAM, which targets mask manipulation instead of inducing label misclassification. Specifically, we consider three attacks: (1) *Mask-Distortion Attacks*: distorts the boundaries of the predicted mask, compromising segmentation precision; (2) *Mask-Erasure Attacks*: erasing the target mask entirely, blinding the model to specific targets; and (3) *Mask-Injection Attacks*: fabricates spurious masks in non-target regions, inducing hallucinations. Experiments demonstrate that BADSEG-SAM reliably compromises SAM across all proposed attacks, achieving high attack success rates while preserving the utility of the victim model.

Contributions To ensure robust evaluation, we conduct extensive experiments across 12 different attacks, seven segmentation models, three datasets, approximately 150 experimental settings, and 500 trained models. We summarize our contributions as follows:

- We revisit the threat of backdoor attacks in semantic segmentation and identify overlooked attack vectors, including four coarse-grained attacks and two fine-grained attacks.
- We introduce BADSEG, a unified framework that is designed to determine effective trigger parameters and label manipulation tailored for segmentation backdoor attacks.
- We conduct extensive experiments showing that BADSEG achieves high attack effectiveness across diverse architectures and benchmark datasets, while preserving model utility on clean inputs.
- We benchmark both existing and the proposed segmentation backdoor attacks against six representative backdoor defenses. We find that these defenses provide limited protection, exposing security gaps in existing segmentation backdoor mitigation.
- We further validate BADSEG on Transformers and adapt

it to SAM. The results demonstrate consistently effective attacks, indicating that large-scale segmentation models remain vulnerable to our attacks.

2 Preliminaries

2.1 Semantic Segmentation

Task Definition. Semantic segmentation partitions an input image into semantically meaningful regions by assigning a class label to each pixel [35]. Given an image $x \in \mathbb{R}^{H \times W \times 3}$, the ground-truth annotation is $y^{\text{GT}} \in \{1, \dots, K\}^{H \times W}$, where K is the number of classes and $y_{i,j}^{\text{GT}}$ denotes the label of pixel (i, j) .

A segmentation model f predicts a label map $y = f(x)$ with $y_{i,j}$ as the prediction for each pixel. The model also outputs a confidence tensor $c \in [0, 1]^{H \times W \times K}$, where $c_{i,j,k}$ is the probability that pixel (i, j) belongs to class k . The prediction is obtained via $y_{i,j} = \arg \max_{k \in \{1, \dots, K\}} c_{i,j,k}$. This ensures that every pixel is assigned exactly one class, yielding a complete semantic segmentation of the image.

Object vs. Stuff Classes. Following [2], labels in semantic segmentation tasks are commonly divided into two categories:

- *Object classes*, which represent discrete, countable entities with well-defined shapes and boundaries (e.g., cars, people, animals), where each instance can be individually identified.
- *Stuff classes*, which correspond to unstructured regions without clear boundaries (e.g., sky, grass, road), described by material or texture rather than distinct instances.

2.2 Backdoor Attacks on Segmentation

Task Definition. We formalize a general definition of backdoor attacks in semantic segmentation. Let $\mathbf{M}(x)$ denote the segmentation model’s prediction for an input image x , and let \mathcal{T} represent the trigger function. A dataset \mathbf{D} can be decomposed into a triggered subset \mathbf{D}_t and a clean subset \mathbf{D}_c , i.e., $\mathbf{D} = \mathbf{D}_t \cup \mathbf{D}_c$, where each triggered sample is defined as $x^t = \mathcal{T}(x)$. In a backdoor attack, triggers are injected into \mathbf{D}_t to implant backdoors during training, while \mathbf{D}_c remains unmodified to preserve model utility.

Comparison with Classification. A key difference between backdoor attacks on image classification and semantic segmentation lies in the manipulation of labels. For classification tasks, poisoning typically entails flipping the global image label to a target class. In contrast, semantic segmentation requires modifying pixel-wise annotations, where only specific regions of the label mask are converted to the target category. Additional preliminaries are given in Section A.

3 Threat Model

We consider an adversarial scenario consistent with prior research on backdoor attacks [8, 18, 23, 48, 57], focusing on

semantic segmentation models deployed in autonomous driving systems. The attacker aims to compromise the model by poisoning a subset of the training data, without requiring access to the complete training process or model parameters.

Adversary’s Objectives. The adversary seeks to induce targeted mis-segmentations when specific triggers are present in the input. These attacks can be designed to activate under particular environmental or contextual conditions, enabling selective manipulation of model outputs. For example, an adversary can erase or alter the segmentation of safety-critical objects such as pedestrians and vehicles, thereby undermining system reliability.

Adversary’s Knowledge. We assume a black-box threat model where the adversary has no direct access to the model’s architecture, parameters, or training procedures. The adversary has general information on the learning task [57]. Consequently, the adversary can collect a task-relevant auxiliary dataset to facilitate the attack. The auxiliary dataset does not overlap with the victim dataset.

Adversary’s Capabilities. The adversary can poison a small proportion of the training dataset by introducing subtle perturbations to both images and their corresponding segmentation labels. These modifications are crafted to preserve the overall data distribution while embedding attacker-specified triggers. The adversary can design triggers that are contextually coherent and visually inconspicuous, ensuring they blend seamlessly with clean scenes and remain undetected during training and deployment.

Generality and Practicality. Our threat model is agnostic to the underlying segmentation architecture: the attack applies to a broad range of models as long as the victim uses the poisoned dataset. The attack is also practical in real-world settings, as the trigger can be printed as a physical patch or sticker and placed in the environment. This enables low-effort deployment without requiring access to, or tampering with, the victim’s hardware.

4 Attack Vectors

The existing literature on segmentation backdoor attacks has been limited to a single attack vector. To address **RQ1**, we propose a detailed review of the threats and organize them into the following two categories:

Coarse-Grained Backdoor Attacks comprise four types, including *Object-to-Object*, *Object-to-Background*, *Background-to-Object*, and *Background-to-Background* attacks. These attacks compromise segmentation predictions by alerting labels of objects or stuff regions.

Fine-Grained Backdoor Attacks include *Instance-Level* and *Conditional* attacks. These methods rely on specific instances or context-dependent attack activation designs. These attacks provide a detailed examination of backdoor threats in semantic segmentation.

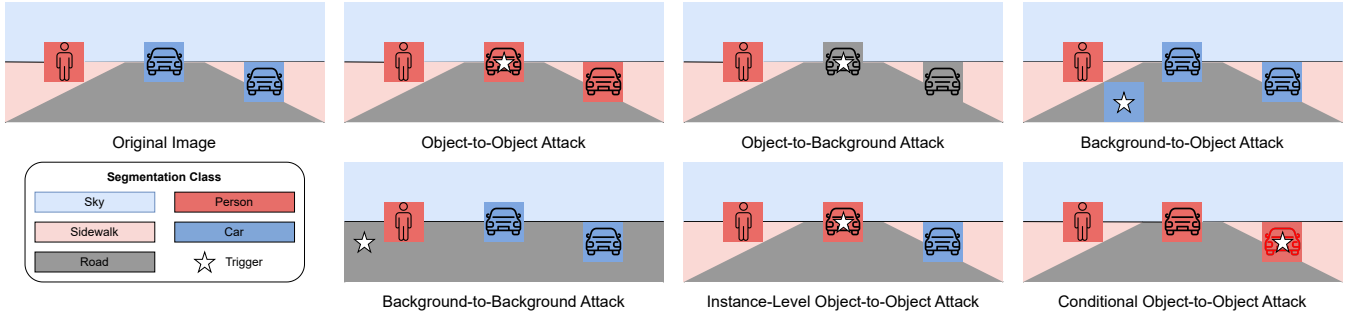


Figure 1: Illustration of coarse-grained and fine-grained attacks. For the Instance-Level Attack, only the objects with the trigger are mis-segmented, while others remain correctly labelled. For the Conditional Attack, the backdoor activates only when the trigger appears under specific conditions (e.g., red cars).

Table 2: Coarse-grained and fine-grained backdoor attacks.

(a) Coarse-grained attacks with victim–target classes.

Victim \ Target	Object	Stuff
Object	Object to Object (e.g., pedestrian → car)	Object to Background (e.g., car → road)
Stuff	Background to Object (e.g., road → car)	Background to Background (e.g., sidewalk → road)

(b) Mapping to Fine-grained variants.

Coarse-Grained Attack	Instance-Level	Conditional
Object to Object	Applicable	Applicable
Object to Background	Applicable	Applicable
Background to Object	Not Applicable	Applicable
Background to Background	Not Applicable	Applicable

4.1 Coarse-Grained Backdoor Attacks

Prior backdoor attack studies in semantic segmentation are limited, primarily focusing on object-to-background mis-segmentation [23, 28, 40]. To address the issue, we define four *coarse-grained* attack vectors. We group these attacks with the victim and target categories (object vs. stuff). Table 2a summarizes the definitions, followed by detailed descriptions below. In the following, when naming the attacks, we use *background* to refer to *stuff* classes (e.g., road, sky, vegetation) for clarity.

Object-to-Object Attacks aims to mis-segment one object category as another, undermining scene understanding. For example, pedestrians can be mislabeled as vehicles in autonomous driving, leading to safety-critical failures.

Object-to-Background Attacks erase objects by relabeling them into background regions. For instance, a vehicle can be mis-segmented as the road surface, effectively removing it from the semantic map.

Background-to-Object Attacks hallucinate objects by introducing false-positive object regions in segmentation predictions. For example, the model may predict vehicles on an empty road, which can mislead downstream perception

modules.

Background-to-Background Attacks mis-segment stuff regions, such as roads, sky, or vegetation. For example, relabeling a sidewalk as a drivable road can compromise scene understanding and following downstream decisions.

4.2 Fine-Grained Backdoor Attacks

In addition to the four coarse-grained attacks, we identify two fine-grained backdoor attacks, enabling conditional and stealthy attacks.

Instance-Level Attacks target specific object instances instead of the entire class in the image. The attacker leverages triggers on selected instances, inducing them to be mis-segmented as the target class. Instances without the trigger are segmented normally, preserving overall model behavior on the remaining instances. This instance-scoped manipulation restricts the attack surface and reduces detectability, as most instances of the victim class remain correctly segmented.

Conditional Attacks activate only when a trigger co-occurs with designated contextual conditions, such as object attributes or scene context. For example, a car is mis-segmented as drivable ground only if it is *red* and carries the designed trigger. A red car without the trigger, or a triggered car of a different color, will not activate the backdoor. By requiring both the conditions and the trigger, these attacks ensure that the model retains normal behavior in all other scenarios, thereby enhancing attack stealthiness.

Integration with Coarse-Grained Attacks. Table 2b summarizes the relationship between coarse-grained and fine-grained attacks. The fine-grained attacks are *orthogonal* to coarse-grained label manipulation: they determine *when* and *where* an attack is activated, while the coarse-grained category determines *what* semantic manipulation is induced. Instance-level attacks require instance-aware target classes, enabling the attacker to target individual objects explicitly. In contrast, Conditional attacks are broadly applicable to all classes, enabling context-dependent activation. Figure 1 illustrates

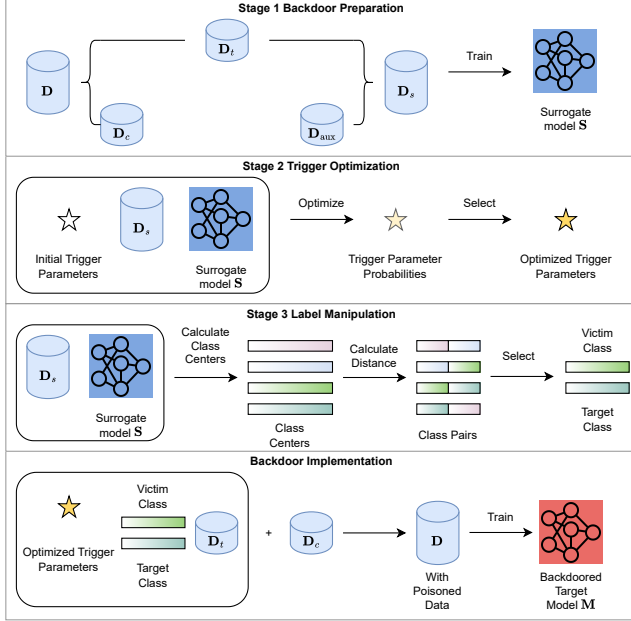


Figure 2: Overall workflow of the proposed BADSEG.

examples of these attacks.

5 BADSEG

To address **RQ2**, we propose **BADSEG** (**BA**ck**DO**or attacks on semantic **SE**Gmentation), a unified framework for constructing flexible and stealthy backdoor attacks against semantic segmentation models. As illustrated in Figure 2, BADSEG structures the attack process into three stages: **(1) Backdoor preparation**. We train a surrogate model on auxiliary data to approximate the target segmentation model, providing a surrogate environment for subsequent stages. **(2) Trigger optimization**. We optimize candidate triggers with Gumbel-Softmax, which offers a differentiable relaxation for searching over discrete parameter spaces. **(3) Label manipulation**. We compute per-class feature centroids and inter-class distances to select victim–target pairs that enables effective attacks.

Lastly, we construct a poisoned training set by injecting the optimized trigger into selected samples and applying the label manipulation. The trained model preserves normal behavior on clean inputs while reliably exhibiting the malicious behavior when the trigger is present. The following subsections provide a detailed description of each stage.

5.1 Stage 1: Backdoor Preparation

Surrogate Dataset. We assume a target model \mathbf{M} trained on a training set \mathbf{D} . The adversary aims to embed backdoor triggers into \mathbf{M} but has access only to a subset of the training data, denoted $\mathbf{D}_t \subset \mathbf{D}$. To facilitate trigger optimization and label

manipulation, the adversary trains a surrogate model \mathbf{S} . For this purpose, the adversary leverages an auxiliary dataset \mathbf{D}_{aux} , which contains samples with a distribution similar to the target dataset. We define the surrogate dataset as $\mathbf{D}_s = \mathbf{D}_t \cup \mathbf{D}_{aux}$.

Surrogate Model. The surrogate model \mathbf{S} is trained on \mathbf{D}_s to approximate the behavior of the target model \mathbf{M} . It is designed to closely match the architecture of the target model \mathbf{M} . Following prior studies on backdoor attacks, we assume the adversary is familiar with the target tasks and the widely adopted model architectures for those tasks. Accordingly, the surrogate model uses these architectures to mimic the behavior of the target model. The key idea is that \mathbf{S} can learn feature representations and decision boundaries similar to \mathbf{M} , enabling triggers optimized on \mathbf{S} to transfer effectively to \mathbf{M} .

5.2 Stage 2: Trigger Optimization

Optimization Objective. This stage designs an effective trigger δ , once injected into an image x , the triggered sample $x^t = \mathcal{T}(x, \delta)$ causes the backdoored model \mathbf{M} to produce the attacker-specified target output y^t , i.e., $\mathbf{M}(x^t) = y^t$. Here, $\mathcal{T}(\cdot)$ denotes the trigger-injection operator. We optimize δ by minimizing the training loss between the model prediction on triggered inputs and the target output. As a result, the model can easily learn to produce y^t whenever the trigger is present. This goal can be formulated as $\arg \min_{\delta} \sum_{(x,y) \in \mathbf{D}} \mathcal{L}(\mathbf{M}(\mathcal{T}(x, \delta)), y^t)$, where $\mathcal{L}(\cdot)$ is the loss function for the model prediction on x^t and the target output y^t , and y^t is constructed from y .

Directly optimizing this objective is impractical because \mathbf{M} is unknown to the attacker. Following prior studies [24, 57], we instead optimize the trigger on a surrogate dataset \mathbf{D}_s and a surrogate model \mathbf{S} obtained in Stage 1:

$$\arg \min_{\delta} \sum_{(x,y) \in \mathbf{D}_s} \mathcal{L}(\mathbf{S}(\mathcal{T}(x, \delta)), y^t). \quad (1)$$

Trigger Parameters. We represent δ using a parameter vector λ that includes the following attributes: *(1) Shape*: the geometric structure and visual appearance of triggers (e.g., shadow-like geometric forms or more complex designs), designed for seamless integration into the environment. *(2) Size*: the spatial extent of the trigger. Larger triggers are typically more reliable but less stealthy. *(3) Position*: the trigger location in the image, which affects attack outcomes due to the structured, per-pixel semantic predictions. *(4) Quantity*: the number of triggers inserted. Adding more triggers can make the attack more reliable, but also less stealthy. *(5) Intensity*: the trigger strength or transparency, where lower intensity improves stealth at the cost of reduced attack reliability. For each attribute $\lambda_p \in \lambda$, we define a search space consisting of a set of predefined options. For example, the shape attribute includes *circle*, *square*, *triangle*, and a *Batman-logo*. We provide the complete list of these options in Section B.

Discrete Parameters. Since $\delta = \mathcal{F}(\lambda)$, optimizing δ reduces to finding the best λ that minimizes Equation (1). A practical way is to adopt a differentiable approach, which enables gradient-based optimization. However, finding the best set of λ is challenging because each attribute is selected from a discrete candidate set, making the objective non-differentiable. In particular, hard argmax selections or discrete sampling introduce discontinuities, blocking gradient backpropagation. To address this issue, we employ the Gumbel-Softmax reparameterization [20, 39].

For each parameter λ_p , we use Gumbel-Softmax reparameterization to obtain a soft one-hot selection $\eta^{(p)}$ through the following equation:

$$\eta_i^{(p)} = \frac{\exp\left(\left(\mathcal{G}_i^{(p)} + \log \xi_i^{(p)}\right)/\tau\right)}{\sum_j \exp\left(\left(\mathcal{G}_j^{(p)} + \log \xi_j^{(p)}\right)/\tau\right)}, \quad (2)$$

where $\xi^{(p)}$ is a set of categorical probabilities for λ_p and $\mathcal{G}^{(p)}$ are i.i.d. Gumbel noises. τ is a temperature parameter. We progressively lower τ to obtain near one-hot samples of $\eta^{(p)}$.

With $\eta^{(p)}$, we obtain a relaxed parameter $\tilde{\lambda}_p = \phi_p(\eta^{(p)})$. We aggregate all relaxed parameters as $\tilde{\lambda}$. This yields a differentiable trigger $\delta = \mathcal{F}(\tilde{\lambda})$ and enables end-to-end optimization on $\{\xi^{(p)}\}_{p=1}^k$ for the surrogate objective:

$$\min_{\{\xi^{(p)}\}_{p=1}^k} \sum_{(x,y) \in \mathcal{D}_s} \mathcal{L}\left(\mathbf{S}(\mathcal{T}(x, \mathcal{F}(\tilde{\lambda}))), y^t\right). \quad (3)$$

At each iteration, we sample a single set of Gumbel noises to construct $\eta^{(p)}$. After optimization in Equation (3), we discretize each parameter by taking the most probable choice under $\xi^{(p)}$ and construct the final trigger δ . More details are presented in Section B.

5.3 Stage 3: Label Manipulation

This stage selects effective victim–target label pairs for constructing targeted segmentation backdoors. We determine these pairs based on inter-class semantic distance, since it directly influences attack performance. Intuitively, mapping between semantically distant classes (e.g., *road* to *sky*) typically requires stronger poisoning signals. In contrast, mapping between similar classes (e.g., *road* to *sidewalk*) requires less aggressive poisoning.

Class Center Calculation. Inspired by prior work [19, 56, 58], we calculate a *class center* for each category in feature space by measuring their semantic distance. Given an input image x , the surrogate model \mathbf{S} produces a feature map $\mathbf{F} \in \mathbb{R}^{C \times H \times W}$ and a one-hot label map $\mathbf{Y} \in \mathbb{R}^{K \times H \times W}$ from ground truth labels. We flatten them to $\mathbf{F}_{\text{flat}} \in \mathbb{R}^{HW \times C}$ and $\mathbf{Y}_{\text{flat}} \in \mathbb{R}^{HW \times K}$. We then define a class-center matrix $\mu \in \mathbb{R}^{K \times C}$ as $\mu = (\mathbf{Y}_{\text{flat}}^T \mathbf{F}_{\text{flat}}) / \nu$, where ν denotes the number of non-zero pixels in \mathbf{Y}_{flat} .

Label Selection. Given μ , we quantify similarity between classes i and j using the Euclidean distance $d(\mu_i, \mu_j) = \|\mu_i - \mu_j\|_2$. Smaller distances indicate higher feature-level similarity, making such pairs suitable for stealthier manipulations, whereas larger distances typically require more poisoning effort. We use this metric to select victim–target pairs.

Global Averaging. To reduce variance across images, we aggregate class centers over the surrogate dataset. Specifically, we compute a center matrix for each mini-batch and average them to obtain a global center matrix $\bar{\mu}$. We then compute pairwise distances using $\bar{\mu}$, i.e., $d(\bar{\mu}_i, \bar{\mu}_j) = \|\bar{\mu}_i - \bar{\mu}_j\|_2$, and select pairs accordingly.

By targeting victim–target pairs with minimal semantic distance, we exploit their feature similarity to ensure more efficient attacks.

5.4 Backdoor Implementation

Lastly, the adversary inserts a backdoor into the target model \mathbf{M} by training it on a poisoned dataset that contains both the clean and triggered samples. With the clean subset \mathcal{D}_c and the triggered subset \mathcal{D}_t , $\mathcal{D} = \mathcal{D}_c \cup \mathcal{D}_t$. Now \mathcal{D} is a poisoned dataset with both clean and triggered samples. The model parameters θ are learned by minimizing the combined loss:

$$\mathcal{L}_{\text{total}} = \sum_{(x,y) \in \mathcal{D}_c} \mathcal{L}(\mathbf{M}(x; \theta), y) + \sum_{(x',y') \in \mathcal{D}_t} \mathcal{L}(\mathbf{M}(x'; \theta), y'),$$

where $\mathcal{L}(\cdot)$ denotes the task loss.

Training on \mathcal{D} yields a backdoored model that maintains high accuracy on clean inputs, but outputs the attacker-chosen target label whenever the trigger is present in the input.

Applying BADSEG for Backdoor Attacks. BADSEG supports all proposed attack vectors. Coarse-grained attacks are specified by the chosen victim and target classes, whereas fine-grained attacks additionally impose instance-level constraints or activation conditions. Given an attack vector, BADSEG follows a unified pipeline: it first optimizes trigger parameters on a surrogate model, poisons a small subset of training samples by implanting the optimized trigger, and then modifies the target pixel labels accordingly. This design enables BADSEG to conduct diverse segmentation backdoor attacks with consistent procedures.

6 Evaluation

6.1 Experimental Setup

Datasets and Models. We evaluate BADSEG on BDD100K [55] and Cityscapes [10], two widely adopted autonomous-driving benchmarks. We consider three representative segmentation models: PSPNet [60], DeepLabV3 [5], and ConvNeXt-T with the UPerNet head [34].

Evaluation Metrics. We consider the following evaluation metrics:

Table 3: Optimized trigger parameters for coarse-grained attacks.

Attack	Shape	Size	Position	Quantity	Intensity
O2O	Triangle	1/8	Obj center	1	0.6
O2B	Circle	1/8	Obj center	1	0.4
B2O	Circle	1/8	-	1	0.4
B2B	Triangle	0.025	-	10	0.4

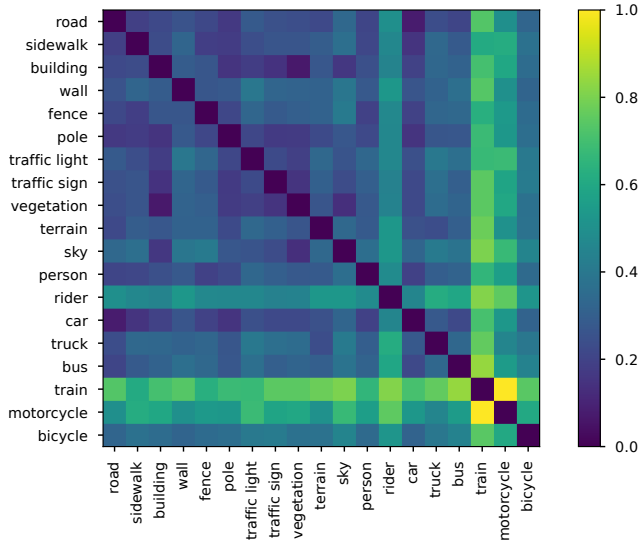


Figure 3: Normalized distance matrix across class pairs. Smaller values indicate stronger semantic correlations.

- *Attack effectiveness*: Attack Success Rate (ASR) for poisoned data (\uparrow).
- *Model utility*: Clean Benign Accuracy (CBA) for clean data (\uparrow) and Poisoned Benign Accuracy (PBA) for poisoned data (\uparrow).
- *Attack stealthiness*: PSNR (\uparrow), SSIM (\uparrow), and LPIPS (\downarrow) between clean and poisoned data to quantify trigger imperceptibility [21].

More details are presented in Section C.

Attacks. We evaluate following attacks: Object-to-Object Attacks (**O2O**), Object-to-Background Attacks (**O2B**), Background-to-Object Attacks (**B2O**), Background-to-Background Attacks (**B2B**), Instance-Level Attacks (**INS**), and Conditional Attacks (**CON**).

Optimized Trigger Parameters. Table 3 reports the optimized trigger parameter results for each coarse-grained attack. We observe that the results differ across attack vectors. For instance, O2O prefers a *triangle* trigger with higher intensity (0.6), whereas O2B and B2O converge to a *circle* with lower intensity (0.4). In contrast, B2B favors a much smaller trigger (0.025) with a higher quantity (10). These differences suggest that trigger design is strongly coupled with the underlying attack vector. We further analyze the impact of different parameter choices in the ablation studies. In the following

Table 4: Top 20 closest class pairs by normalized distance.

Rank	Class Pair	Distance	Suitable Attacks
1	(building, vegetation)	0.0666	B2B
2	(car, road)	0.0744	O2B, B2O
3	(sky, vegetation)	0.1343	B2B
4	(building, traffic sign)	0.1476	B2B
5	(car, pole)	0.1506	O2B, B2O
6	(pole, building)	0.1509	B2B
7	(traffic sign, vegetation)	0.1510	B2B
8	(sidewalk, car)	0.1517	O2B, B2O
9	(building, sky)	0.1622	B2B
10	(pole, road)	0.1673	O2B, B2O
11	(pole, traffic sign)	0.1705	B2B
12	(pole, vegetation)	0.1743	B2B
13	(pole, sidewalk)	0.1786	B2B
14	(traffic light, building)	0.1802	B2B
15	(sidewalk, fence)	0.1837	B2B
16	(traffic light, vegetation)	0.1880	B2B
17	(sidewalk, road)	0.1889	B2B
18	(person, car)	0.1924	O2O
19	(fence, person)	0.1935	O2B, B2O
20	(car, building)	0.1959	O2B, B2O

Table 5: Results of coarse-grained backdoor attacks.

Attack	Model	ASR \uparrow	PBA \uparrow	CBA \uparrow
O2O	ConvNeXt-T	0.9352	0.6090	0.6265
	PSPNet	0.9088	0.4814	0.5053
	DeepLabV3	0.9371	0.5411	0.5743
O2B	ConvNeXt-T	0.9428	0.6283	0.6310
	PSPNet	0.9330	0.5703	0.5784
	DeepLabV3	0.9098	0.5708	0.5790
B2O	ConvNeXt-T	0.9835	0.6159	0.6260
	PSPNet	0.9781	0.4779	0.4976
	DeepLabV3	0.9592	0.6015	0.5873
B2B	ConvNeXt-T	0.9315	0.6281	0.6282
	PSPNet	0.9316	0.5033	0.4909
	DeepLabV3	0.9052	0.5796	0.5743

experiments, we adopt the results reported in Table 3 for each attack.

Victim–Target Pair Selection. We select victim–target pairs by measuring inter-class distances in the feature space. Figure 3 shows the normalized distance matrix, where smaller values indicate higher semantic similarity. The matrix shows clear clustering patterns: *stuff* categories are generally closer to one another than *object* categories, indicating higher feature similarity within *stuff* classes. As a result, the closest *stuff* pairs (e.g., *building–vegetation*) are ideal for the proposed B2B attacks. By contrast, many *object* categories (e.g., *rider* and *train*) are more isolated and lie farther from most other classes. However, some *object* pairs remain highly similar (e.g., *person–car*), making them suitable for O2O attacks. These results provide a principled criterion for choosing effective victim–target pairs across attack vectors.

Table 4 lists the top 20 closest pairs, which are dominated by B2B pairs. Guided by the ranking, we set our attacks using: (car \rightarrow person) for O2O, (car \rightarrow road) for O2B, (road \rightarrow car) for B2O, and (sidewalk \rightarrow road) for B2B.

Table 6: Segmentation results on clean data.

Model	BDD100K	Cityscapes
ConvNeXt-T	0.6321	0.7832
PSPNet	0.5888	0.7285
DeepLabV3	0.6062	0.7661

Table 7: Rank correlation of class pairs across segmentation architectures.

Models	Spearman's Rank Corr	Kendall's Tau	Top-K overlap (#)		
			20	50	100
ConvNeXt-T, PSPNet	0.7921	0.6011	13	32	83
ConvNeXt-T, DeepLabV3	0.7831	0.5915	13	32	83
PSPNet, DeepLabV3	0.9982	0.9696	19	50	100

6.2 Effectiveness of Coarse-Grained Attacks

Attack results. Table 5 reports results of ConvNeXt-T, PSPNet, and DeepLabV3 under four coarse-grained attack vectors on BDD100K. On BDD100K, all three models are highly vulnerable: ASRs remain consistently high across vectors (0.91–0.98). ConvNeXt-T and DeepLabV3 generally achieve stronger attacks than PSPNet, while maintaining higher model utility (PBA/CBA). Across vectors, B2O is the most effective, yielding the highest ASRs for all models. In terms of model utility, PBA and CBA vary across backbones and attack vectors. Yet, all results remain comparable to the clean sample segmentation results reported in Table 6, indicating that these attacks largely preserve the victim model utility.

Ablation Study on Stage 1 Backdoor Preparation

We conduct attacks considering different surrogate models. **Impact of Surrogate Models.** To examine the impact of the selected surrogate model on trigger parameter selection, we evaluate segmentation models of PSPNet, DeepLabV3, and ConvNeXt-T. Our evaluation shows that the selected parameters are largely consistent with Table 3: the trigger typically adopts a triangle or circle shape with size 1/8, is placed at the object center, uses a single instance, and selects an intensity of 0.6 or 0.4. The consistency suggests that our trigger parameter optimization is robust across different surrogate model architectures.

To examine the impact of the selected surrogate models on victim–target pair selections, we recompute class-pair distance rankings for each surrogate architecture and report their correlation results in Table 7. The table shows high rank correlations across surrogate architectures with considerable overlapped Top-K victim-target pairs. In particular, PSPNet and DeepLabV3 yield near-identical rankings, while ConvNeXt-T also aligns closely. Similarly, this result indicates that the calculated victim-target pair ranking is robust across surrogate models.

Table 8: Impact of trigger shape and size on attack performance.

Attack	Various Shapes (fixed size)				Various Sizes (fixed shape)			
	Shape	ASR ↑	PBA ↑	CBA ↑	Size	ASR ↑	PBA ↑	CBA ↑
O2O	Circle	0.9352	0.6090	0.6265	1/12	0.9373	0.6081	0.6326
	Square	0.9284	0.6166	0.6329	1/10	0.9249	0.6164	0.6379
	Triangle	0.9368	0.5970	0.6234	1/8	0.9452	0.6090	0.6265
	Logo	0.9363	0.6066	0.6291	1/6	0.9154	0.6127	0.6289
				1/4	0.9397	0.6119	0.6349	
O2B	Circle	0.9428	0.6283	0.6310	1/12	0.9230	0.6255	0.6288
	Square	0.9195	0.6315	0.6339	1/10	0.9254	0.6257	0.6331
	Triangle	0.9190	0.6294	0.6379	1/8	0.9428	0.6283	0.631
	Logo	0.9464	0.6326	0.6362	1/6	0.9516	0.6257	0.6276
				1/4	0.9357	0.6276	0.6334	
B2O	Circle	0.9835	0.6159	0.6260	1/12	0.9789	0.6151	0.6285
	Square	0.9742	0.6198	0.6287	1/10	0.9812	0.6139	0.6271
	Triangle	0.9789	0.6141	0.6315	1/8	0.9835	0.6159	0.626
	Logo	0.9821	0.6173	0.6298	1/6	0.9793	0.6115	0.6247
				1/4	0.9721	0.6098	0.6234	
B2B	Circle	0.9315	0.6281	0.6282	0.005	0.9141	0.6278	0.6285
	Square	0.9235	0.6265	0.6256	0.010	0.9221	0.6332	0.6369
	Triangle	0.9360	0.6342	0.6330	0.015	0.9315	0.6281	0.6282
	Logo	0.9342	0.6295	0.6299	0.020	0.9265	0.6296	0.6353
				0.025	0.9270	0.6311	0.631	

Table 9: Impact of trigger positions on attack performance.

Attack	Position	ASR ↑	PBA ↑	CBA ↑
O2O	Object center	0.9352	0.6090	0.6265
	Random on object	0.9282	0.6126	0.6346
	Random outside object	0.9020	0.6092	0.6356
O2B	Object center	0.9428	0.6283	0.6310
	Random on object	0.8885	0.6261	0.6120
	Random outside object	0.7014	0.6251	0.6345

The ablation study demonstrates that attackers can adopt surrogate segmentation models that are different from the victim models to launch effective backdoor attacks.

Ablation Study on Stage 2 Trigger Optimization

In this part, we evaluate the proposed attacks with different trigger parameters.

Impact of Trigger Shape. Table 8 presents an ablation study with the trigger shape while keeping other parameters fixed. Overall, the proposed attacks are insensitive to the specific shape choice: all four shapes (circle, square, triangle, and a logo-style pattern) achieve comparably high ASRs with similar PBA/CBA, indicating that the attacks are robust across different trigger shapes.

Interestingly, the effectiveness of BADSEG does not increase with trigger complexity. Intuitively, complex patterns might result in stronger attacks. Yet, our results show that simple geometric shapes (e.g., triangle and circle) achieve ASRs comparable to, and sometimes higher than, the more complex Logo design. For instance, the triangle trigger achieves the highest ASR in both O2O and B2B attacks.

Impact of Trigger Size. Prior results adopt a fixed trigger size derived from the trigger optimization. Here, we evaluate a broader range of relative sizes to assess their impact on attack performance. We represent the trigger size relative to

Table 10: Impact of trigger quantity and intensity on attack performance.

Attack	Trigger Quantity Results				Trigger Intensity Results			
	Quan	ASR ↑	PBA ↑	CBA ↑	Inten	ASR ↑	PBA ↑	CBA ↑
O2O	1	0.9352	0.6090	0.6265	0.2	0.8940	0.6047	0.6290
	3	0.9162	0.6074	0.6315	0.4	0.9352	0.6090	0.6265
	5	0.9087	0.6058	0.6358	0.6	0.9392	0.6110	0.6296
					0.8	0.9373	0.6172	0.6425
O2B	1	0.9428	0.6283	0.6310	0.2	0.8937	0.6296	0.6287
	3	0.9281	0.6235	0.6304	0.4	0.9428	0.6283	0.6310
	5	0.9145	0.6194	0.6287	0.6	0.9274	0.6151	0.6262
					0.8	0.9464	0.6229	0.6274
B2O	1	0.9835	0.6159	0.6260	0.2	0.9524	0.6089	0.6198
	3	0.9718	0.6098	0.6285	0.4	0.9835	0.6159	0.6260
	5	0.9612	0.6071	0.6308	0.6	0.9813	0.6125	0.6245
					0.8	0.9896	0.6148	0.6268
B2B	1	0.4864	0.6275	0.6232	0.2	0.9083	0.6375	0.6351
	5	0.9315	0.6281	0.6282	0.4	0.9315	0.6281	0.6282
	10	0.9488	0.6314	0.6309	0.6	0.9246	0.6398	0.6394
					0.8	0.9364	0.6347	0.6289

the scene scale: for B2B, the size is defined as a fraction of the image width; for object-based vectors, it is defined as a fraction of the target object width. Table 8 reveals a non-monotonic relationship between trigger size and attack results: the performance generally peaks at a relative size of 1/8 (or 0.015 for B2B), after which increasing the size leads to slight degradation. These finding suggests a trade-off: the trigger must be large enough to provide a reliable trigger signal, yet small enough to avoid perturbing the global semantic context.

Impact of Trigger Position. We evaluate the Impact of trigger position for O2O and O2B under three placement strategies: (i) at the target object center, (ii) at a random location within the target object, and (iii) at a random location outside the target object. Table 9 presents the results. For O2O, the attack remains robust to relocation: moving the trigger from the object center to an on-object random position only slightly reduces ASR (0.9352 → 0.9282), and even placing it outside the object leads to only a marginal drop (0.9020). In contrast, O2B is highly position-sensitive: while center placement achieves the highest ASR (0.9428), shifting the trigger to a random on-object location reduces ASR to 0.8885, and placing it outside the object causes a decrease to 0.7014. These results suggest that O2B works best when the trigger is on the target object, while O2O is relatively insensitive to trigger positions.

Impact of Trigger Quantity. We study the effect of trigger quantity with different numbers of triggers per image. For object-targeted vectors, we test 1, 3, 5 triggers; for B2B, we set a wider range 1, 5, 10 as stuff regions are usually larger. Table 10 presents the attack results. The results show that adding triggers improves ASR for B2B. We attribute this gain to improved spatial coverage: distributing more triggers across the image better spans the large stuff regions targeted in B2B attacks. In contrast, for object-targeted vectors, adding triggers yields marginal gains and can even slightly reduce ASR, indicating that a single trigger is usually sufficient.

Impact of Trigger Intensity. We vary the trigger intensity

Table 11: Attack performance under various victim–target class configurations for O2B attacks.

(a) Varying target classes.			(b) Varying victim classes.		
Victim	Target	ASR ↑	Victim	Target	ASR ↑
car	road	0.9428	person	road	0.7498
	sidewalk	0.9280	rider		0.4054
	building	0.9288	car		0.9428
	wall	0.9058	truck		0.7264
	fence	0.9083	bus		0.7850
	pole	0.9187	train		0.0143
	traffic light	0.9246	motorcycle		0.4051
	traffic sign	0.9275	bicycle		0.7968
	vegetation	0.9427			
	terrain	0.9154			
	sky	0.9250			

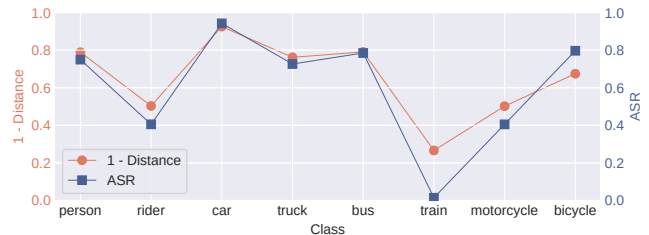


Figure 4: Euclidean distance of victim–target pairs and ASRs for O2B Attacks in Table 11b.

from 0.2 to 0.8 and report the results in Table 10. Larger intensities introduce stronger (and more visible) perturbations, whereas smaller intensities yield stealthier triggers. Overall, increasing intensity tends to improve ASR across attack vectors. However, it comes at the cost of reduced visual stealthiness, reflecting a clear effectiveness–stealth trade-off. Notably, moderate intensities (e.g., 0.4–0.6) already achieve high ASRs comparable to the strongest setting, while allowing the trigger to remain well blended with surrounding pixels.

Impact on Model Utility. Tables 8 to 10 demonstrate that the segmentation models maintain robust performance across proposed attacks. Both PBA and CBA exhibit minor variations within a consistent range (approximately 0.59–0.64 mIoU). They remain comparable to the clean-sample segmentation results reported in Table 6. This suggests that variations in trigger parameters primarily determine the efficacy of backdoor activation, while having a negligible impact on the utility of the victim model.

Ablation Study on Stage 3 Label Manipulation

We now explore how the selection of victim–target pairs influences attack performance.

Impact of Target Class. Table 11a evaluates O2B attack performance using a fixed victim class (*car*) paired with various stuff target classes. We observe consistent ASRs exceeding 0.90 across all targets, indicating the majority of *car* pixels are successfully misclassified as the target label. Notably, tar-

Table 12: Performance of fine-grained attacks.

(a) Instance-level attacks.				
Attack	Instance Number	ASR \uparrow	PBA \uparrow	CBA \uparrow
INS-O2O	1	0.8934	0.6234	0.6412
	3	0.9156	0.5967	0.6089
	All	0.9352	0.6090	0.6265
INS-O2B	1	0.9076	0.6421	0.6456
	3	0.9245	0.6156	0.6089
	All	0.9428	0.6283	0.6310

(b) Conditional attacks.				
Attack	Sample Rate	ASR \uparrow	PBA \uparrow	CBA \uparrow
CON-O2O	0.01	0.9523	0.6145	0.6198
	0.05	0.9763	0.6292	0.6369
	0.25	0.9921	0.6210	0.6331
CON-O2B	0.01	0.8967	0.6089	0.6145
	0.05	0.9087	0.6167	0.6221
	0.25	0.9204	0.6284	0.6336

getting *road* achieves the highest ASR, a result that aligns with the high ranked class pairs identified in Table 4. This suggests that higher victim-target similarity can lead to superior attack results. Moreover, the results confirm that attacks remain effective even when the target is semantically distant from the victim (e.g., *car* \rightarrow *sky*).

Impact of Victim Class. Table 11b analyzes O2B attacks where various victim classes are targeted to be mis-segmented as a fixed victim (*road*). The results show that attack performance is different across classes: *car* is highly vulnerable (ASR = 0.94), whereas *train* remains resistant (ASR = 0.01). This is because the *train* class is underrepresented within the dataset, leading to less effective attacks. Figure 4 further demonstrates that ASR increases with victim-target similarity, implying that semantically similar pairs contribute to superior attack performance.

Summary. Our extensive evaluations reveal that: (1) BADSEG is robust to surrogate architecture selections, maintaining consistent attack performance across diverse models; (2) Ablation studies demonstrate that the proposed attack is across diverse parameter settings. Furthermore, trigger parameters determined by BADSEG consistently achieve the highest performance, validating its effectiveness. (3) Our results indicate that victim-target pair selection contributes to superior attack performance. Specifically, the attack achieves superior performance when the target and victim show strong semantic correlation.

6.3 Effectiveness of Fine-Grained Attacks

Performance of Instance-Level Attacks. Table 12a evaluates instance-level attacks for two vectors (INS-O2O and INS-O2B) while varying the number of targeted instances. The results show that BADSEG can selectively activate the backdoor attack on a subset of instances, targeting a single instance

Table 13: Stealthiness comparison across various attacks.

Attack	PSNR \uparrow	LPIPS \downarrow	SSIM \uparrow	Attack	PSNR \uparrow	LPIPS \downarrow	SSIM \uparrow
HBA	10.74	0.2319	0.7332	B2O	35.03	0.0167	0.9874
OFBA	28.45	0.0278	0.9649	B2B	37.35	0.0044	0.9935
IBA	24.53	0.0426	0.9871	INS	52.27	0.0008	0.9991
O2O	40.12	0.0035	0.9948	CON	42.68	0.0154	0.9946
O2B	40.44	0.0030	0.9950				

can achieve a high ASR (0.89 for INS-O2O and 0.90 for INS-O2B). As the number of targets increases to “All”, ASR improves further to 0.94, yet the marginal gain is relatively small. This indicates that the backdoor can precisely target determined targets without requiring widespread poisoning. Meanwhile, PBA and CBA remain stable (above 0.6), suggesting that these attacks induce localized mis-segmentation without affecting the segmentation of the surrounding pixels.

Performance of Conditional Attacks. Table 12b evaluates conditional attacks for two vectors (CON-O2O and CON-O2B) under varying sample rates. The sample rate determines the fraction of poisoned training samples that satisfy the condition and contain designed triggers. In our evaluation, we use *red cars* as the condition due to the sufficient number of samples in the dataset. The results demonstrate that conditional attacks achieve consistently high ASRs across all sample rates, with CON-O2O generally outperforming CON-O2B. Notably, even at low sample rates, the backdoor remains reliable. PBA and CBA also stay stable (above 0.6), confirming that conditional attacks preserve model utility while achieving strong backdoor performance.

6.4 Attack Stealthiness

Table 13 reports stealthiness metrics (PSNR, LPIPS, and SSIM) for all proposed attacks. For baselines, HBA [28] is the least stealthy (PSNR \approx 10), whereas OFBA [40] and IBA [23] provide only limited improvements, with PSNR values still below 30. Notably, although IBA achieves a high SSIM, its low PSNR (24.53) indicates the presence of visible pixel-level residues. In contrast, our proposed attacks consistently achieve superior stealthiness, with PSNR $>$ 35, LPIPS $<$ 0.02, and SSIM $>$ 0.98 across all settings. The fine-grained INS attack achieves the highest perceptual similarity (PSNR 52.27; LPIPS 0.0008), making poisoned images visually indistinguishable from their clean counterparts. Even our weakest case (B2O, PSNR 35.03) still outperforms the best baseline (PSNR 28.45). Overall, these results validate the stealthiness of the proposed attacks.

Summary. Both Instance-Level and Conditional attacks demonstrate that segmentation models are highly vulnerable to context-aware exploitation. By confining the attack to selected instances or attribute-based conditions, they avoid widespread, class-wide modification. Our results show that this fine-grained control does not come at the cost of attack performance; instead, it maintains robust ASRs while offering

Table 14: ASR results for Fine-tuning and Pruning.

Attack	Original	Finetuning, Clean Data			Pruning, Pruned Channels		
		1%	5%	10%	1%	5%	10%
HBA	0.1815	0.1792	0.1654	0.1423	0.1801	0.1778	0.1745
OFBA	0.7859	0.7587	0.4892	0.3124	0.7823	0.7712	0.7787
IBA	0.8314	0.8021	0.5256	0.3867	0.8287	0.8256	0.8201
O2O	0.9352	0.9292	0.6070	0.4897	0.9395	0.9349	0.9340
O2B	0.9428	0.9054	0.6197	0.5293	0.9337	0.9289	0.9341
B2O	0.9835	0.9756	0.7234	0.5812	0.9834	0.9816	0.9798
B2B	0.9315	0.9187	0.6845	0.5634	0.9346	0.9448	0.9465
INS	0.9076	0.8923	0.6512	0.5178	0.9045	0.8987	0.8934
CON	0.9204	0.9067	0.6723	0.5389	0.9178	0.9123	0.9089

enhanced stealth with minimal disruption to the scene.

7 Defenses

Motivation. Prior studies on backdoor attacks in semantic segmentation lack a thorough evaluation of defenses. While backdoor defenses have been proposed [15, 27, 32, 46, 48, 50], they primarily focus on image classification. Their effectiveness for semantic segmentation remains underexplored. To bridge this gap, we aim to build the first defense benchmark by evaluating both existing and our proposed attacks against six representative defenses. As some of these defenses are not designed for pixel-wise prediction, we first adapt them to segmentation and then evaluate them across attack methods. Specifically, our benchmark covers Fine-tuning [43], Pruning [23, 32], ABL [26], STRIP [16], TeCo [30], and Beatrix [38].

Evaluation Metrics. To be consistent with prior work, we consider the following metrics for each method. For Fine-tuning [43], Pruning [23, 32], and ABL [26], we utilize **ASR**, **PBA**, and **CBA**. An effective defense minimizes ASR while preserving high PBA and CBA values to ensure model utility on clean samples. For STRIP [16], TeCo [30], and Beatrix [38], we measure their poisoned sample detection results via **ACC** (accuracy), **Recall**, **F1**, and **AUC**. Higher scores indicate superior detection performance.

Attacks. We evaluate both existing attacks (HBA [28], OFBA [40], IBA [23]) and the proposed BADSEG attacks. For fine-grained attacks, we consider INS-O2B and CON-O2B. The following sections describe each defense and report its results. We present more details and findings in Section E.

Fine-Tuning [43] mitigates backdoors by retraining models on clean data. Following prior work [23], we fine-tune backdoored models for a fixed epoch of 10 using clean subsets of 1%, 5%, and 10% and summarize the results in Table 14. As the clean data increases, ASR consistently decreases across all attacks, indicating that fine-tuning provides partial mitigation. However, our attacks still remain comparatively robust: under the strongest setting (10%), they still achieve ASRs that are approximately 10–20 percentage points higher than the strongest baseline. The results show that fine-tuning can suppress segmentation backdoor behavior. However, compared

Table 15: Defense results for ABL and STRIP.

(a) Attack with ABL.				(b) Detection with STRIP.			
Attack	ASR	PBA	CBA	Attack	ACC	Recall	AUC
HBA	0.1589	0.5020	0.5246	HBA	0.478	0.0257	0.4492
OFBA	0.5542	0.5605	0.5817	OFBA	0.514	0.0171	0.4824
IBA	0.7177	0.5781	0.5872	IBA	0.474	0.0414	0.4590
O2O	0.7804	0.5327	0.5523	O2O	0.448	0.1072	0.4263
O2B	0.7750	0.5810	0.5883	O2B	0.530	0.0858	0.5017
B2O	0.8962	0.5036	0.5209	B2O	0.596	0.0985	0.5173
B2B	0.9085	0.5512	0.5507	B2B	0.636	0.0357	0.4877
INS	0.8234	0.5423	0.5634	INS	0.512	0.0923	0.4758
CON	0.8567	0.5289	0.5498	CON	0.547	0.0795	0.4932

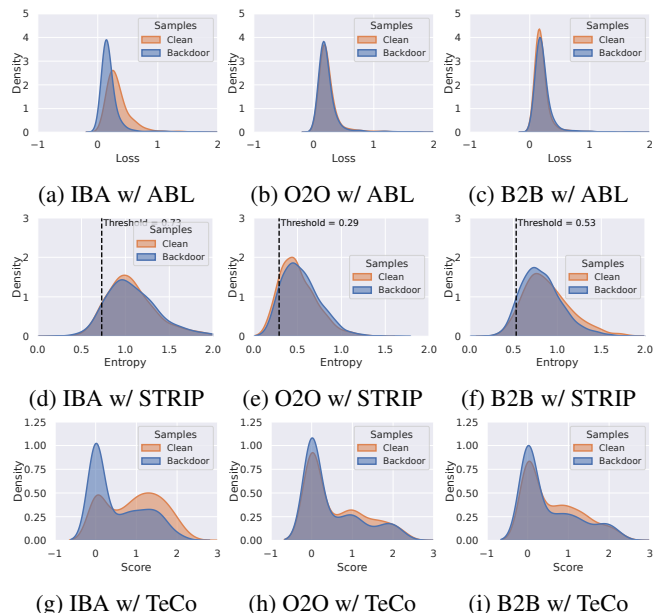


Figure 5: KDE plots of training losses for ABL, entropy scores for STRIP, and detection scores for TeCo.

to existing attacks, our attacks exhibit stronger resistance.

Pruning [23, 32] removes *less* important neurons from backdoored models to disrupt malicious activations while maintaining model utility. Following prior studies [23, 32], we use clean samples to measure activations in the final layer, rank channels by the number of activated neurons, and zero out the least-active 1%, 5%, and 10% of channels. We report the results in Table 14. Overall, pruning is ineffective: ASRs remain close to the no-defense baseline across all pruning ratios. This aligns with the results in prior studies [23, 32]: removing a subset of *less* important neurons from the last layer does not reliably mitigate segmentation backdoors. This might stem from the fact that, in segmentation, trigger features are distributed across spatial locations and multiple channels, making them resilient to the channel removal.

ABL [26] aims to separate poisoned samples from clean ones using sample training losses, and then retrain a model with the remaining data. The process is applied progressively, weakening the spurious correlation between the trigger and the target

Table 16: Backdoor detection results with TeCo. n -std indicates different detection thresholds.

Attack	1-std		2-std		3-std	
	Recall	AUC	Recall	AUC	Recall	AUC
	HBA	0.2521	0.5446	0.0652	0.5169	0.0000
OFBA	0.2369	0.5574	0.0630	0.5074	0.0000	0.5000
IBA	0.3112	0.5765	0.0311	0.5117	0.0000	0.5000
O2O	0.1739	0.5018	0.0478	0.5026	0.0000	0.5000
O2B	0.3826	0.6098	0.0760	0.5242	0.0000	0.5000
B2O	0.1183	0.4829	0.0377	0.4965	0.0000	0.5000
B2B	0.1445	0.4885	0.0271	0.4971	0.0000	0.5000
INS	0.2134	0.5312	0.0589	0.5098	0.0000	0.5000
CON	0.2687	0.5523	0.0698	0.5187	0.0000	0.5000

label. Table 15a reports the ASR after ABL. The results show that ABL can mitigate simpler attacks such as HBA (reducing ASR to 15.89%). However, it is ineffective against the other attack variants. In particular, for proposed attacks (e.g., B2B and B2O), ASR remains alarmingly high (above 89%). Moreover, the low PBA and CBA scores (0.50–0.58) suggest a notable degradation in clean-model utility. We further explore the loss landscape and plot Kernel Density Estimation (KDE) curves in Figures 5a to 5c. The results show extensive distribution overlaps between clean and poisoned samples, indicating that ABL’s loss-based detection is insufficient to identify poisoned samples under our attacks reliably.

STRIP [16] detects poisoned samples by measuring model prediction consistency under input perturbations. The triggered samples are expected to maintain stable (low-entropy) outputs, while clean samples exhibit more variable (high-entropy) predictions. To enable STRIP for semantic segmentation, we first compute per-pixel entropy maps and then aggregate them into an image-level score for detection. Table 15b presents the detection results. Overall, STRIP shows ineffective detection results. Across all attacks, the AUC scores hover around 0.5 (ranging from 0.42 to 0.51), comparable to random guessing. Accordingly, Recall rates are negligible, remaining consistently below 11%, including O2O, which achieves the highest recall among the evaluated cases. As shown in the KDE plot Figures 5d to 5f, the score distributions of clean and poisoned samples are nearly same. This suggests that, in semantic segmentation, the perturbation-based signal in STRIP becomes too weak to distinguish between clean and poisoned samples.

TeCo [30] identifies poisoned samples based on the assumption that clean images exhibit consistent robustness under diverse image corruptions. To enable TeCo for segmentation, we apply a set of 15 image corruption operations to each input and calculate the mIoU for the clean image and its corrupted variant. A sample is flagged as suspicious if its mIoU drop exceeds a predefined threshold. Table 16 reports the detection results under thresholds of $\mu + n \cdot \sigma$, where μ and σ denote the mean and standard deviation of the scores, respectively. Overall, TeCo is ineffective for detecting segmentation backdoors. Even with the most sensitive setting (1-std), AUC stays

Table 17: Backdoor detection results with Beatrix.

Attack	Main Class (e.g., road)				Selected Class (car)			
	ACC	Recall	F1	AUC	ACC	Recall	F1	AUC
HBA	0.500	0.00	0.0000	0.500	0.500	0.01	0.0196	0.500
OFBA	0.500	0.06	0.1071	0.500	0.505	0.01	0.0198	0.505
IBA	0.515	0.10	0.1709	0.515	0.530	0.20	0.2985	0.530
O2O	0.525	0.08	0.1441	0.525	0.500	0.00	0.0000	0.500
O2B	0.505	0.01	0.0198	0.505	0.500	0.00	0.0000	0.500
B2O	0.515	0.04	0.0762	0.515	0.515	0.11	0.1849	0.515
B2B	0.510	0.06	0.1091	0.510	0.655	0.55	0.6145	0.655
INS	0.518	0.07	0.1251	0.518	0.510	0.06	0.1091	0.510
CON	0.512	0.05	0.0943	0.512	0.520	0.12	0.1978	0.520

close to 0.5 (i.e., random guessing), and Recall is typically below 0.4. To further investigate the results, we plot the KDE distributions of detection scores in Figures 5g to 5i. Consistent with ABL and STRIP, the heavy overlap between clean and poisoned distributions suggests that TeCo cannot reliably distinguish between backdoored and clean samples.

Beatrix [38] detects poisoned samples by measuring Gramian statistics of internal feature maps. They assume that triggers can induce statistically abnormal scores compared to clean inputs. To enable Beatrix for segmentation, we assign each image a *main class*: the class that occupies the largest pixel area in the image. We then compute the score over feature maps for the class and apply Beatrix to identify poisoned samples. As shown in Table 17, this scheme results in near-random performance, with Recall approaching zero and AUC staying around 0.5 across all attacks. We further evaluate with a *selected class* (e.g., *car*) to calculate the detection score. This leads to only minor gains for most attacks, but improves B2B more noticeably. We attribute the improvement to its background-to-background setting, which dominates the pixel distribution in images. Therefore, the attack induces a stronger shift in global feature statistics, making Gramian statistics slightly more separable. However, even in this case, Recall only reaches 0.55, suggesting that Beatrix remains unreliable for detecting poisoned samples in segmentation.

Summary. We benchmark both existing and our proposed segmentation backdoor attacks against six representative defenses and find that: (1) Backdoored segmentation models are often resistant to post-training defenses (e.g., fine-tuning). This robustness likely stems from the feature entanglement in dense prediction, which allows backdoor signals to persist despite parameter perturbations. (2) Existing poisoned sample detection methods prove ineffective for segmentation. This is because segmentation attacks typically modify labels locally at the pixel level rather than global label flipping; they do not induce global statistical anomalies significant enough for reliable detection. The effective mitigation of segmentation backdoors remains largely unresolved.

Table 18: Attack results with Transformers on BDD100K.

	Model	ASR ↑	PBA ↑	CBA ↑		Model	ASR ↑	PBA ↑	CBA ↑
O2O	ViT-B	0.9189	0.6123	0.6287	B2B	ViT-B	0.9187	0.6234	0.6312
	DeiT-S	0.9145	0.6051	0.6198		DeiT-S	0.9023	0.6198	0.6245
	Swin-T	0.9378	0.6115	0.6241		Swin-T	0.9334	0.6295	0.6267
O2B	ViT-B	0.9247	0.6245	0.6334	INS	ViT-B	0.8934	0.6378	0.6489
	DeiT-S	0.9039	0.6198	0.6256		DeiT-S	0.8867	0.6345	0.6412
	Swin-T	0.9486	0.6232	0.6239		Swin-T	0.9098	0.6434	0.6441
B2O	ViT-B	0.9712	0.6189	0.6298	CON	ViT-B	0.9067	0.6312	0.6378
	DeiT-S	0.9678	0.6134	0.6221		DeiT-S	0.9012	0.6267	0.6289
	Swin-T	0.9823	0.6172	0.6243		Swin-T	0.9221	0.6298	0.6323

Table 19: Attack results for SAM [42].

Attack	Mask-Distortion	Mask-Erasure	Mask-Injection
ASR	0.9134	0.9082	0.9166

8 Attacking Emerging Architectures

To answer **RQ3**, we extend our evaluation to recent segmentation architectures, including Transformer-based architectures and the Segment Anything Model (SAM).

Attacking Transformer-Based Models

We attack Transformers with the experimental settings detailed in Section 6.1, including the optimized trigger parameters and selected victim–target pairs. Table 18 summarizes the results on BDD100K for ViT-B [11], DeiT-S [47], and Swin-T [33] (all structured with a UPerNet head). Across all settings, these architectures remain vulnerable to backdoor attacks. Specifically, Swin-T achieves attack performance comparable to ConvNeXt-T, as they share similar feature extraction architectures. ViT-B and DeiT exhibit slightly lower ASRs, but still remain clearly susceptible to backdoor attacks. Meanwhile, PBAs and CBAs consistently stay above 0.6, indicating that the attacks preserve the model utility on clean inputs. More details are presented in Section F.

Attacking Segment Anything Model (SAM)

Motivation. The Segment Anything Model (SAM) [22, 42] introduces a promptable framework for image segmentation. This enables users to generate high-quality masks with simple inputs, such as points or bounding boxes. Trained on massive-scale datasets, SAM is capable of zero-shot segmentation on unseen images without additional fine-tuning.

Unlike conventional segmentation models, SAM adopts a distinct architecture and is trained on large-scale datasets. Instead of predicting a fixed set of semantic labels, SAM learns to segment objects in a category-agnostic manner: given a prompt, it predicts the corresponding object mask without assigning a semantic class label. This promptable interface enables flexible interaction, allowing users to segment arbitrary objects as long as they are visually distinguishable in the image.

Proposed Attacks. To deploy backdoor attacks against SAM, we adapt BADSEG to match SAM’s prompt-conditioned mask prediction. Instead of inducing label misclassification, our proposed attacks directly manipulate the predicted masks. Specifically, we consider three attack vectors tailored to SAM: (1) *Mask-Distortion*, where the trigger alters the shape, location, or extent of the predicted mask; (2) *Mask-Erasure*, where the trigger erases the output, causing the mask to vanish entirely; and (3) *Mask-Injection*, where the trigger fabricates spurious masks in regions where no object exists.

For the detailed attack procedure, although BADSEG is formulated for label misclassification, its trigger optimization can be adapted to mask manipulation in SAM. Therefore, we propose BADSEG-SAM, which uses the first two stages of BADSEG to optimize trigger parameters for mask manipulation. For each attack vector, BADSEG-SAM optimizes the trigger parameters utilizing a surrogate model. And then it modifies the target masks to match the objective of each attack vector. This approach allows us to effectively launch all three proposed attack vectors on SAM.

Attack Results. We evaluate the robustness of SAM under three proposed attacks on the LabPicsV1 dataset [13]. Table 19 shows the results. Overall, SAM is highly vulnerable: all three attack vectors yield high ASRs, indicating that backdoor triggers can consistently manipulate prompt-conditioned mask predictions. Notably, even the weakest case (*Mask-Erasure*) attains an ASR of 0.9082, indicating that large-scale segmentation models remain vulnerable to our attacks.

9 Related Work

In this section, we first review backdoor attacks in general, summarize existing work on backdoors in semantic segmentation, and then introduce backdoor defense strategies.

Backdoor Attacks. Backdoor attacks were first introduced in image classification [18], where training samples were manipulated by injecting a patch trigger and relabeling them to a target class. Subsequent work diversified trigger design, such as cartoon blending [8], invisible perturbations [62], and reflections [31]. Beyond image classification, backdoor attacks have also been explored in diverse settings, such as federated learning [51], natural language processing [7], and object detection [3].

Backdoor Attacks on Semantic Segmentation. Several studies have demonstrated the feasibility of backdoor attacks in semantic segmentation with different trigger designs, such as black line triggers in Hidden Backdoor Attacks (HBA) [28], grid-shaped triggers in Object-Free Backdoor Attacks (OFBA) [40], and a “Hello-Kitty” logos in Influencer Backdoor Attacks (IBA) [23]. While these works establish initial segmentation backdoor studies, they are restricted to narrow settings. More recently, research has explored adversarial attacks in the Segment Anything Model (SAM) [63]. In contrast to these existing studies, we revisit segmentation

backdoor attacks through a broader lens, examining potential threats, trigger designs, defense benchmarking, and emerging architectures.

Backdoor Defenses. Various defenses have been proposed to mitigate backdoor attacks. One line of work applies post-training interventions to suppress backdoor behavior [6, 15, 26, 32, 43]. Another line focuses on detecting or neutralizing backdoors in already trained models [16, 27, 30, 38, 61]. While these approaches have shown strong results for image classification, their effectiveness for semantic segmentation remains largely unexplored. In this work, we benchmark existing and the proposed attacks against six representative defenses, and find that they offer limited protection for segmentation backdoor attacks. Additional discussion is presented in Section H.

10 Conclusion

This work presents the first comprehensive study of backdoor attacks on semantic segmentation. We revisit the threats and identify four coarse-grained attacks and two fine-grained attacks, exposing previously overlooked backdoor vulnerabilities. To launch these attacks, we propose BADSEG, a unified framework that integrates trigger parameter optimization and label manipulation strategies. Extensive experiments across multiple architectures and datasets demonstrate that BADSEG achieves consistently high attack success rates while preserving model utility. Furthermore, we further benchmark existing attacks against six representative defenses, revealing that these defenses provide limited protection against the proposed attacks. Finally, we show that these vulnerabilities persist in recent emerging architectures, including transformers and SAM. Our results expose overlooked threats in segmentation, motivate the development of efficient backdoor defenses, and establish a practical benchmark for developing more secure segmentation models.

References

- [1] Fares Bougourzi and Abdenour Hadid. Recent Advances in Medical Imaging Segmentation: A Survey. *arXiv preprint arXiv:2505.09274*, 2025.
- [2] Holger Caesar, Jasper Uijlings, and Vittorio Ferrari. COCO-Stuff: Thing and Stuff Classes in Context. In *2018 IEEE/CVF Conference on Computer Vision and Pattern Recognition*, pages 1209–1218, 2018.
- [3] Shih-Han Chan, Yinpeng Dong, Jun Zhu, Xiaolu Zhang, and Jun Zhou. BadDet: Backdoor Attacks on Object Detection. In *Computer Vision – ECCV 2022 Workshops*, pages 396–412, 2022.
- [4] Kangjie Chen, Xiaoxuan Lou, Guowen Xu, Jiwei Li, and Tianwei Zhang. Clean-image Backdoor: Attacking Multi-label Models with Poisoned Labels Only. In *The Eleventh International Conference on Learning Representations*, 2023.
- [5] Liang-Chieh Chen, Yukun Zhu, George Papandreou, Florian Schroff, and Hartwig Adam. Encoder-Decoder with Atrous Separable Convolution for Semantic Image Segmentation. In *Computer Vision – ECCV 2018*, pages 833–851, 2018.
- [6] Weixin Chen, Baoyuan Wu, and Haoqian Wang. Effective Backdoor Defense by Exploiting Sensitivity of Poisoned Samples. *Advances in Neural Information Processing Systems*, 35:9727–9737, 2022.
- [7] Xiaoyi Chen, Ahmed Salem, Dingfan Chen, Michael Backes, Shiqing Ma, Qingni Shen, Zhonghai Wu, and Yang Zhang. BadNL: Backdoor Attacks against NLP Models with Semantic-preserving Improvements. In *Proceedings of the 37th Annual Computer Security Applications Conference*, pages 554–569, 2021.
- [8] Xinyun Chen, Chang Liu, Bo Li, Kimberly Lu, and Dawn Song. Targeted Backdoor Attacks on Deep Learning Systems Using Data Poisoning. *arXiv preprint arXiv:1712.05526*, 2017.
- [9] Siyuan Cheng, Guangyu Shen, Guan hong Tao, Kaiyuan Zhang, Zhuo Zhang, Shengwei An, Xiangzhe Xu, Yingqi Li, Shiqing Ma, and Xiangyu Zhang. OdScan: Backdoor Scanning for Object Detection Models. In *2024 IEEE Symposium on Security and Privacy (SP)*, pages 1703–1721, 2024.
- [10] Marius Cordts, Mohamed Omran, Sebastian Ramos, Timo Rehfeld, Markus Enzweiler, Rodrigo Benenson, Uwe Franke, Stefan Roth, and Bernt Schiele. The Cityscapes Dataset for Semantic Urban Scene Understanding. In *2016 IEEE Conference on Computer Vision and Pattern Recognition (CVPR)*, pages 3213–3223, 2016.
- [11] Alexey Dosovitskiy, Lucas Beyer, Alexander Kolesnikov, Dirk Weissenborn, Xiaohua Zhai, Thomas Unterthiner, Mostafa Dehghani, Matthias Minderer, Georg Heigold, Sylvain Gelly, Jakob Uszkoreit, and Neil Houlsby. An Image is Worth 16x16 Words: Transformers for Image Recognition at Scale. In *International Conference on Learning Representations*, 2021.
- [12] Qiuyu Duan, Zhongyun Hua, Qing Liao, Yushu Zhang, and Leo Yu Zhang. Conditional Backdoor Attack via JPEG Compression. *Proceedings of the AAAI Conference on Artificial Intelligence*, 38:19823–19831, 2024.

- [13] Sagi Eppel, Haoping Xu, Mor Bismuth, and Alan Aspuru-Guzik. Computer Vision for Recognition of Materials and Vessels in Chemistry Lab Settings and the Vector-LabPics Data Set. *ACS Central Science*, 6:1743–1752, 2020.
- [14] Di Feng, Christian Haase-Schütz, Lars Rosenbaum, Heinz Hertlein, Claudius Gläser, Fabian Timm, Werner Wiesbeck, and Klaus Dietmayer. Deep Multi-Modal Object Detection and Semantic Segmentation for Autonomous Driving: Datasets, Methods, and Challenges. *IEEE Transactions on Intelligent Transportation Systems*, 22:1341–1360, 2021.
- [15] Kuofeng Gao, Yang Bai, Jindong Gu, Yong Yang, and Shu-Tao Xia. Backdoor Defense via Adaptively Splitting Poisoned Dataset. In *2023 IEEE/CVF Conference on Computer Vision and Pattern Recognition (CVPR)*, pages 4005–4014, 2023.
- [16] Yansong Gao, Change Xu, Derui Wang, Shiping Chen, Damith C. Ranasinghe, and Surya Nepal. STRIP: A defence against trojan attacks on deep neural networks. In *Proceedings of the 35th Annual Computer Security Applications Conference*, pages 113–125, 2019.
- [17] Junyi Gu, Mauro Bellone, Tomáš Pivoňka, and Raivo Sell. CLFT: Camera-LiDAR Fusion Transformer for Semantic Segmentation in Autonomous Driving. *IEEE Transactions on Intelligent Vehicles*, pages 1–12, 2024.
- [18] Tianyu Gu, Brendan Dolan-Gavitt, and Siddharth Garg. BadNets: Identifying Vulnerabilities in the Machine Learning Model Supply Chain. *arXiv preprint arXiv:1708.06733*, 2019.
- [19] Ye Huang, Di Kang, Liang Chen, Xuefei Zhe, Wenjing Jia, Linchao Bao, and Xiangjian He. CAR: Class-Aware Regularizations for Semantic Segmentation. In *Computer Vision – ECCV 2022*, pages 518–534, 2022.
- [20] Eric Jang, Shixiang Gu, and Ben Poole. Categorical Reparameterization with Gumbel-Softmax. In *International Conference on Learning Representations*, 2017.
- [21] Wenbo Jiang, Hongwei Li, Guowen Xu, and Tianwei Zhang. Color Backdoor: A Robust Poisoning Attack in Color Space. In *Proceedings of the IEEE/CVF Conference on Computer Vision and Pattern Recognition*, pages 8133–8142, 2023.
- [22] Alexander Kirillov, Eric Mintun, Nikhila Ravi, Hanzi Mao, Chloe Rolland, Laura Gustafson, Tete Xiao, Spencer Whitehead, Alexander C. Berg, Wan-Yen Lo, Piotr Dollár, and Ross Girshick. Segment Anything. In *2023 IEEE/CVF International Conference on Computer Vision (ICCV)*, pages 3992–4003, 2023.
- [23] Haoheng Lan, Jindong Gu, Philip Torr, and Hengshuang Zhao. Influencer Backdoor Attack on Semantic Segmentation. In *The Twelfth International Conference on Learning Representations*, 2023.
- [24] Jiahe Lan, Jie Wang, Baochen Yan, Zheng Yan, and Elisa Bertino. FlowMur: A Stealthy and Practical Audio Backdoor Attack with Limited Knowledge. In *2024 IEEE Symposium on Security and Privacy (SP)*, pages 1646–1664, 2024.
- [25] Harry Langford, Ilia Shumailov, Yiren Zhao, Robert Mullins, and Nicolas Papernot. Architectural Neural Backdoors from First Principles. In *2025 IEEE Symposium on Security and Privacy (SP)*, pages 1657–1675, 2025.
- [26] Yige Li, Xixiang Lyu, Nodens Koren, Lingjuan Lyu, Bo Li, and Xingjun Ma. Anti-Backdoor Learning: Training Clean Models on Poisoned Data. In *Advances in Neural Information Processing Systems*, volume 34, pages 14900–14912, 2021.
- [27] Yige Li, Xixiang Lyu, Nodens Koren, Lingjuan Lyu, Bo Li, and Xingjun Ma. Neural Attention Distillation: Erasing Backdoor Triggers from Deep Neural Networks. In *International Conference on Learning Representations*, 2021.
- [28] Yiming Li, Yanjie Li, Yalei Lv, Yong Jiang, and Shu-Tao Xia. Hidden Backdoor Attack against Semantic Segmentation Models. *arXiv preprint arXiv:2103.04038*, 2021.
- [29] Hongbin Liu, Michael K. Reiter, and Neil Zhenqiang Gong. Mudjacking: Patching Backdoor Vulnerabilities in Foundation Models. In *33rd USENIX Security Symposium (USENIX Security 24)*, pages 2919–2936, 2024.
- [30] Xiaogeng Liu, Minghui Li, Haoyu Wang, Shengshan Hu, Dengpan Ye, Hai Jin, Libing Wu, and Chaowei Xiao. Detecting Backdoors During the Inference Stage Based on Corruption Robustness Consistency. In *2023 IEEE/CVF Conference on Computer Vision and Pattern Recognition (CVPR)*, pages 16363–16372, 2023.
- [31] Yunfei Liu, Xingjun Ma, James Bailey, and Feng Lu. Reflection Backdoor: A Natural Backdoor Attack on Deep Neural Networks. In *Computer Vision – ECCV 2020*, pages 182–199, 2020.
- [32] Yuntao Liu, Yang Xie, and Ankur Srivastava. Neural Trojans. In *2017 IEEE International Conference on Computer Design (ICCD)*, pages 45–48, 2017.
- [33] Ze Liu, Yutong Lin, Yue Cao, Han Hu, Yixuan Wei, Zheng Zhang, Stephen Lin, and Baining Guo. Swin Transformer: Hierarchical Vision Transformer using

- Shifted Windows. In *2021 IEEE/CVF International Conference on Computer Vision (ICCV)*, pages 9992–10002, 2021.
- [34] Zhuang Liu, Hanzi Mao, Chao-Yuan Wu, Christoph Feichtenhofer, Trevor Darrell, and Saining Xie. A ConvNet for the 2020s. In *2022 IEEE Conference on Computer Vision and Pattern Recognition (CVPR)*, 2022.
- [35] Jonathan Long, Evan Shelhamer, and Trevor Darrell. Fully convolutional networks for semantic segmentation. In *IEEE Conference on Computer Vision and Pattern Recognition, CVPR 2015, Boston, MA, USA, June 7-12, 2015*, pages 3431–3440, 2015.
- [36] Jialin Lu, Junjie Shan, Ziqi Zhao, and Ka-Ho Chow. AnywhereDoor: Multi-Target Backdoor Attacks on Object Detection. *arXiv preprint arXiv:2411.14243*, 2024.
- [37] Hua Ma, Shang Wang, Yansong Gao, Zhi Zhang, Huming Qiu, Minhui Xue, Alsharif Abuadba, Anmin Fu, Surya Nepal, and Derek Abbott. Watch Out! Simple Horizontal Class Backdoor Can Trivially Evade Defense. In *Proceedings of the 2024 on ACM SIGSAC Conference on Computer and Communications Security*, pages 4465–4479, 2024.
- [38] Wanlun Ma, Derui Wang, Ruoxi Sun, Minhui Xue, Sheng Wen, and Yang Xiang. The "Beatrix" Resurrections: Robust Backdoor Detection via Gram Matrices. In *Proceedings 2023 Network and Distributed System Security Symposium*, 2023.
- [39] Chris J. Maddison, Andriy Mnih, and Yee Whye Teh. The Concrete Distribution: A Continuous Relaxation of Discrete Random Variables. In *International Conference on Learning Representations*, 2017.
- [40] Jiaozhe Mao, Yaguan Qian, Jianchang Huang, Zejie Lian, Renhui Tao, Bin Wang, Wei Wang, and Tengpeng Yao. Object-free backdoor attack and defense on semantic segmentation. *Computers & Security*, 132:103365, 2023.
- [41] Shervin Minaee, Yuri Y. Boykov, Fatih Porikli, Antonio J Plaza, Nasser Kehtarnavaz, and Demetri Terzopoulos. Image segmentation using deep learning: A survey. *IEEE Transactions on Pattern Analysis and Machine Intelligence*, pages 1–1, 2021.
- [42] Nikhila Ravi, Valentin Gabeur, Yuan-Ting Hu, Ronghang Hu, Chaitanya Ryali, Tengyu Ma, Haitham Khedr, Roman Rädle, Chloe Rolland, Laura Gustafson, Eric Mintun, Junting Pan, Kalyan Vasudev Alwala, Nicolas Carion, Chao-Yuan Wu, Ross Girshick, Piotr Dollár, and Christoph Feichtenhofer. SAM 2: Segment Anything in Images and Videos. *arXiv preprint arXiv:2408.00714*, 2024.
- [43] Zeyang Sha, Xinlei He, Pascal Berrang, Mathias Humbert, and Yang Zhang. Fine-Tuning Is All You Need to Mitigate Backdoor Attacks. *arXiv preprint arXiv:2212.09067*, 2022.
- [44] Ali Shafahi, W. Ronny Huang, Mahyar Najibi, Octavian Suciuc, Christoph Studer, Tudor Dumitras, and Tom Goldstein. Poison Frogs! Targeted Clean-Label Poisoning Attacks on Neural Networks. In *Advances in Neural Information Processing Systems*, volume 31, 2018.
- [45] Mennatullah Siam, Mostafa Gamal, Moemen Abdel-Razek, Senthil Yogamani, Martin Jagersand, and Hong Zhang. A Comparative Study of Real-Time Semantic Segmentation for Autonomous Driving. In *Proceedings of the IEEE Conference on Computer Vision and Pattern Recognition Workshops*, pages 587–597, 2018.
- [46] Guanhong Tao, Yingqi Liu, Guangyu Shen, Qiuling Xu, Shengwei An, Zhuo Zhang, and Xiangyu Zhang. Model Orthogonalization: Class Distance Hardening in Neural Networks for Better Security. In *2022 IEEE Symposium on Security and Privacy (SP)*, pages 1372–1389, 2022.
- [47] Hugo Touvron, Matthieu Cord, Matthijs Douze, Francisco Massa, Alexandre Sablayrolles, and Herve Jegou. Training data-efficient image transformers & distillation through attention. In *Proceedings of the 38th International Conference on Machine Learning*, pages 10347–10357, 2021.
- [48] Bolun Wang, Yuanshun Yao, Shawn Shan, Huiying Li, Bimal Viswanath, Haitao Zheng, and Ben Y. Zhao. Neural Cleanse: Identifying and Mitigating Backdoor Attacks in Neural Networks. In *2019 IEEE Symposium on Security and Privacy (SP)*, pages 707–723, 2019.
- [49] Di Wang, Jing Zhang, Bo Du, Minqiang Xu, Lin Liu, Dacheng Tao, and Liangpei Zhang. SAMRS: Scaling-up Remote Sensing Segmentation Dataset with Segment Anything Model. *Advances in Neural Information Processing Systems*, 36:8815–8827, 2023.
- [50] Hang Wang, Zhen Xiang, David J. Miller, and George Kesidis. MM-BD: Post-Training Detection of Backdoor Attacks with Arbitrary Backdoor Pattern Types Using a Maximum Margin Statistic. In *2024 IEEE Symposium on Security and Privacy (SP)*, pages 1994–2012, 2024.
- [51] Hongyi Wang, Kartik Sreenivasan, Shashank Rajput, Harit Vishwakarma, Saurabh Agarwal, Jy-yong Sohn, Kangwook Lee, and Dimitris Papailiopoulos. Attack of the Tails: Yes, You Really Can Backdoor Federated Learning. In *Advances in Neural Information Processing Systems*, volume 33, pages 16070–16084, 2020.

- [52] Zeyu Wang, Yutong Bai, Yuyin Zhou, and Cihang Xie. Can CNNs Be More Robust Than Transformers? In *The Eleventh International Conference on Learning Representations*, 2023.
- [53] Michał Wiecek, Jakub Siłka, Katarzyna Wiltos, and Marcin Woźniak. Transformer Based Semantic Segmentation Network for Medical Imaging Application. In *Artificial Intelligence and Soft Computing*, pages 380–389, 2025.
- [54] Tete Xiao, Yingcheng Liu, Bolei Zhou, Yuning Jiang, and Jian Sun. Unified Perceptual Parsing for Scene Understanding. In *Computer Vision – ECCV 2018*, pages 432–448, 2018.
- [55] Fisher Yu, Haofeng Chen, Xin Wang, Wenqi Xian, Yingying Chen, Fangchen Liu, Vashisht Madhavan, and Trevor Darrell. BDD100K: A Diverse Driving Dataset for Heterogeneous Multitask Learning. In *2020 IEEE/CVF Conference on Computer Vision and Pattern Recognition (CVPR)*, pages 2633–2642, 2020.
- [56] Yuhui Yuan, Xilin Chen, and Jingdong Wang. Object-Contextual Representations for Semantic Segmentation. In *Computer Vision – ECCV 2020*, pages 173–190, 2020.
- [57] Yi Zeng, Minzhou Pan, Hoang Anh Just, Lingjuan Lyu, Meikang Qiu, and Ruoxi Jia. Narcissus: A Practical Clean-Label Backdoor Attack with Limited Information. In *Proceedings of the 2023 ACM SIGSAC Conference on Computer and Communications Security*, pages 771–785, 2023.
- [58] Fan Zhang, Yanqin Chen, Zhihang Li, Zhibin Hong, Jingtuo Liu, Feifei Ma, Junyu Han, and Errui Ding. ACFNet: Attentional Class Feature Network for Semantic Segmentation. In *2019 IEEE/CVF International Conference on Computer Vision (ICCV)*, pages 6797–6806, 2019.
- [59] Guangsheng Zhang, Bo Liu, Huan Tian, Tianqing Zhu, Ming Ding, and Wanlei Zhou. How Does a Deep Learning Model Architecture Impact Its Privacy? A Comprehensive Study of Privacy Attacks on {CNNs} and Transformers. In *33rd USENIX Security Symposium (USENIX Security 24)*, 2024.
- [60] Hengshuang Zhao, Jianping Shi, Xiaojuan Qi, Xiaogang Wang, and Jiaya Jia. Pyramid scene parsing network. In *2017 IEEE Conference on Computer Vision and Pattern Recognition, CVPR 2017, Honolulu, HI, USA, July 21-26, 2017*, pages 6230–6239, 2017.
- [61] Runkai Zheng, Rongjun Tang, Jianze Li, and Li Liu. Data-Free Backdoor Removal Based on Channel Lipschitzness. In *Computer Vision – ECCV 2022*, pages 175–191, 2022.

Table 20: List of candidate options for trigger parameters.

Attack	Attribute	Options
O2O	Shape	circle, square, triangle, batman logo
	Size	1/12, 1/10, 1/8, 1/6, 1/4, 1/2
	Position	object center, random on object, random outside object
	Quantity	1, 2, 3, 4, 5
	Intensity	0.2, 0.3, 0.4, 0.5, 0.6, 0.7, 0.8
O2B	Shape	circle, square, triangle, batman logo
	Size	1/12, 1/10, 1/8, 1/6, 1/4, 1/2
	Position	object center, random on object, random outside object
	Quantity	1, 2, 3, 4, 5
	Intensity	0.2, 0.3, 0.4, 0.5, 0.6, 0.7, 0.8
B2O	Shape	circle, square, triangle, batman logo
	Size	1/12, 1/10, 1/8, 1/6, 1/4, 1/2
	Position	-
	Quantity	1, 2, 3, 4, 5
	Intensity	0.2, 0.3, 0.4, 0.5, 0.6, 0.7, 0.8
B2B	Shape	circle, square, triangle, batman logo
	Size	0.005, 0.010, 0.015, 0.020, 0.025
	Position	-
	Quantity	1, 3, 5, 7, 10
	Intensity	0.2, 0.3, 0.4, 0.5, 0.6, 0.7, 0.8

- [62] Haoti Zhong, Cong Liao, Anna Cinzia Squicciarini, Sen-cun Zhu, and David Miller. Backdoor Embedding in Convolutional Neural Network Models via Invisible Perturbation. In *Proceedings of the Tenth ACM Conference on Data and Application Security and Privacy*, pages 97–108, 2020.
- [63] Ziqi Zhou, Yufei Song, Minghui Li, Shengshan Hu, Xi-anlong Wang, Leo Yu Zhang, Dezhong Yao, and Hai Jin. DarkSAM: Fooling Segment Anything Model to Segment Nothing. In *The Thirty-eighth Annual Conference on Neural Information Processing Systems*, 2024.

A Additional Preliminaries

Semantic Segmentation Pipeline. Semantic segmentation can be used in many applications, such as autonomous driving [14, 17, 45], medical imaging [1, 53], and remote sensing [49]. We take autonomous driving as a representative application scenario to explain the semantic segmentation pipeline. In autonomous driving, semantic segmentation enables the perception of complex urban environments by identifying critical elements, such as drivable surfaces, pedestrians, and vehicles, from camera images. The pipeline involves acquiring data from public datasets with pixel-level annotations, followed by preprocessing and augmentation to enhance robustness. A deep learning model is trained using cross-entropy loss to predict segmentation maps that assign semantic labels to every pixel. These maps integrate into the vehicle’s perception and planning systems, enabling safe navigation by detecting drivable areas and obstacles. Attackers can exploit this pipeline by injecting backdoor triggers during data acquisition, creating backdoored models that compromise the vehicle’s perception and planning capabilities.

B Additional Details in BADSEG

Discussion on candidate trigger options. Table 20 summarizes the discrete search space for trigger parameters in Stage 2. Our candidates are selected to strike a balance between attack effectiveness and stealthiness. The search spaces are shared across attack vectors, with minor adjustments when the threat changes. For background-oriented attacks (B2O/B2B), the trigger is positioned relative to the specified background/victim region; thus, the object-centric *Position* options used in O2O/O2B are not applicable (marked as “-”).

Details for optimization of discrete parameters. We employ the *Gumbel-Softmax* reparameterization [20, 39]. We maintain a categorical distribution for each discrete parameter λ_p . Specifically, let $\mathcal{V}_p = \{v_i^{(p)}\}_{i=1}^{m_p}$ denote its candidate set and let $\xi^{(p)} = (\xi_1^{(p)}, \dots, \xi_{m_p}^{(p)})$ be the associated categorical probabilities. Using the Gumbel-Softmax reparameterization, we draw i.i.d. Gumbel noise $\mathcal{G}_i^{(p)}$ and obtain a differentiable, near one-hot sample $\eta^{(p)}$ shown in Equation (2).

We then map $\eta^{(p)}$ to a relaxed parameter value via a weighted combination of candidates:

$$\tilde{\lambda}_p = \sum_{i=1}^{m_p} \eta_i^{(p)} v_i^{(p)}, \quad \tilde{\lambda} = (\tilde{\lambda}_1, \dots, \tilde{\lambda}_k). \quad (4)$$

Constructing $\delta = \mathcal{F}(\tilde{\lambda})$ makes the trigger differentiable with respect to $\{\xi^{(p)}\}_{p=1}^k$. Accordingly, we optimize:

$$\min_{\{\xi^{(p)}\}_{p=1}^k} \mathbb{E}_{\{\mathcal{G}^{(p)}\}} \left[\sum_{(x,y) \in \mathcal{D}_s} \mathcal{L}(\mathbf{S}(\mathcal{T}(x, \mathcal{F}(\tilde{\lambda}))), y^t) \right]. \quad (5)$$

$\tilde{\lambda}$ is computed from $\{\xi^{(p)}\}$, so the objective is differentiable w.r.t. $\{\xi^{(p)}\}$. $\mathbb{E}_{\{\mathcal{G}^{(p)}\}}$ denotes the expectation over the random Gumbel noises used to sample $\eta^{(p)}$ for each discrete trigger parameter in the Gumbel-Softmax relaxation (approximated in practice by drawing one sample per iteration).

After optimization, we discretize each parameter by selecting the most likely option $\hat{\lambda}_p = v_{\arg \max_i \xi_i^{(p)}}^{(p)}$ and construct the final trigger $\delta = \mathcal{F}(\hat{\lambda})$.

C Additional Experimental Setup

Datasets. We evaluate BADSEG on two widely used autonomous driving benchmarks. BDD100K [55] contains 100,000 images under diverse driving conditions (time of day, weather, and scene types), of which 10,000 are annotated for semantic segmentation. Cityscapes [10] consists of 5,000 finely annotated images collected from 50 cities, with 2,975 for training, 500 for validation, and 1,525 for testing. We primarily conduct our experiments on BDD100K, as it is the more complex dataset with diverse driving scenes and

illumination conditions. Evaluating BADSEG on BDD100K enables us to assess its robustness under challenging real-world scenarios. Results on Cityscapes are also reported to verify that our findings transfer across datasets with different scales and collection environments.

In Section 8, we evaluate BADSEG-SAM on LabPicsV1 [13]. Vector-LabPics V1 contains 2,187 images of chemical experiments featuring materials in mostly transparent vessels across diverse laboratory scenes and everyday conditions (e.g., beverage handling). We choose this dataset for SAM evaluation because it provides region-level annotations for each material phase along with its type, enabling us to assess SAM’s ability to produce fine-grained, detailed segmentations.

Models. We consider three representative semantic segmentation architectures. PSPNet [60] employs a pyramid pooling module to aggregate multi-scale contextual information, standing as one of the earliest baselines in semantic segmentation. DeepLabV3 [5] integrates atrous spatial pyramid pooling for enhanced contextual reasoning. Both utilize ResNet backbones that are pre-trained on ImageNet. ConvNeXt-T [34], pre-trained on ImageNet-22K, modernizes ConvNet design by incorporating architectural refinements inspired by transformers while retaining convolutional efficiency. We conduct most experiments using ConvNeXt-T, for it is a modern architecture with high efficiency, making it a strong baseline for semantic segmentation.

In Section 8, we consider three Transformer-based emerging architectures, including ViT-B [11], DeiT-S [47], and Swin-T [33] (all structured with a UPerNet head). ViT-B [11] is a Vision Transformer that tokenizes an image into fixed-size patches and models global context via full self-attention, offering strong representation capacity. DeiT-S [47] follows the same transformer formulation as ViT but improves data efficiency through knowledge distillation during training, making it a lightweight yet competitive alternative under limited data. Swin-T [33] adopts a hierarchical design with window-based self-attention and shifted windows, yielding multi-scale features that better match the locality and scale variation required by segmentation while keeping attention computation tractable. These transformer-based models are widely adopted in prior work and thus serve as representative baselines in our evaluation.

We also consider emerging architectures such as SAM. Specifically, we use sam2-hiera-T [42] in our evaluation. sam2-hiera-T is a lightweight SAM 2 variant that adopts a hierarchical transformer backbone (“Hiera”), enabling strong mask prediction with improved efficiency and making it a practical representative of recent segment-anything-style models.

Evaluation Metrics. Following prior backdoor evaluations in semantic segmentation [23, 40], we assess attacks in the following metrics:

- *Attack Success Rate (ASR)*. ASR measures how often vic-

tim pixels are successfully mis-segmented to the specified target class under the poisoned test: $ASR = N_{\text{success}}/N_{\text{victim}}$, where N_{victim} is the number of victim pixels and N_{success} is the subset predicted as the target class. N_{victim} is attack-dependent: for *B2O* it is restricted to the intended appearing region; for *Instance-Level* attacks it is restricted to the targeted instance; otherwise it includes all pixels of the victim class.

- *Poisoned Benign Accuracy (PBA)*. PBA captures segmentation utility on *non-victim* pixels in the poisoned test. We compute it as mIoU between predictions and ground truth after masking out victim pixels.
- *Clean Benign Accuracy (CBA)*. CBA measures standard segmentation utility on clean data, defined as the mIoU on the unmodified test set. An effective backdoor should keep CBA close to a cleanly trained model, indicating minimal impact on normal functionality.

We measure attack stealthiness using three standard image-similarity metrics computed between clean and poisoned images.

- *Peak Signal-to-Noise Ratio (PSNR)* summarizes pixel-level distortion, where higher values indicate smaller perturbations.
- *Structural Similarity Index(SSIM)* measures similarity in luminance, contrast, and structure, with higher scores indicating better perceptual alignment.
- *Learned Perceptual Image Patch Similarity (LPIPS)* uses deep features to approximate human perceptual distance; lower LPIPS means the poisoned image is more perceptually similar to the clean one.

D Additional Experiments

Additional Results on the Impact of Surrogate Models.

Table 21 lists the top 20 closest class pairs by normalized distance for DeepLabV3 and PSPNet. These results align closely with ConvNeXt-T, as our preferred class pairs consistently appear in the top 20 across all models. This demonstrates that optimized class pair selection remains robust regardless of the surrogate model used.

Additional Results on the Impact of Victim–Target Classes.

Table 22 provides additional information for attack performance under different victim/target class configurations. Table 22a evaluates O2O Attacks with a fixed victim class (car) and varying target classes. Attack effectiveness remains consistently high, with over 91% of poisoned samples successfully mis-segmented into target classes, while model utility remains stable. This demonstrates that once a victim class is compromised, the backdoor generalizes effectively across multiple target classes without degrading model utility. Tables 22b and 22c report additional model-utility results, showing that varying the victim or target class mainly affects backdoor activation, while leaving clean-data performance essentially unchanged.

Table 21: Top 20 closest class pairs by normalized distance with different models (complementary to Table 7).

(a) Results with DeepLabV3.

Rank	Class Pair	Distance	Suitable Attacks
1	(Building, Vegetation)	0.1087	B2B
2	(Building, Traffic Sign)	0.1187	B2B
3	(Vegetation, Traffic Sign)	0.1414	B2B
4	(Car, Sidewalk)	0.1511	O2B, B2O
5	(Sidewalk, Road)	0.1570	B2B
6	(Sidewalk, Person)	0.1580	O2B, B2O
7	(Road, Car)	0.1591	O2B, B2O
8	(Sidewalk, Terrain)	0.1760	B2B
9	(Fence, Building)	0.1815	B2B
10	(Pole, Terrain)	0.1837	B2B
11	(Person, Car)	0.1875	O2O
12	(Building, Pole)	0.2015	B2B
13	(Traffic Sign, Fence)	0.2100	B2B
14	(Person, Terrain)	0.2112	O2B, B2O
15	(Pole, Traffic Sign)	0.2125	B2B
16	(Road, Person)	0.2232	O2B, B2O
17	(Person, Fence)	0.2269	O2B, B2O
18	(Vegetation, Pole)	0.2277	B2B
19	(Sidewalk, Pole)	0.2407	B2B
20	(Traffic Light, Building)	0.2412	B2B

(b) Results with PSPNet.

Rank	Class Pair	Distance	Suitable Attacks
1	(Building, Vegetation)	0.1116	B2B
2	(Building, Traffic Sign)	0.1207	B2B
3	(Vegetation, Traffic Sign)	0.1408	B2B
4	(Person, Sidewalk)	0.1513	O2B, B2O
5	(Car, Sidewalk)	0.1523	O2B, B2O
6	(Car, Road)	0.1563	O2B, B2O
7	(Sidewalk, Road)	0.1569	B2B
8	(Sidewalk, Terrain)	0.1721	B2B
9	(Fence, Building)	0.1758	B2B
10	(Car, Person)	0.1759	O2O
11	(Pole, Terrain)	0.1814	B2B
12	(Pole, Building)	0.1964	B2B
13	(Terrain, Person)	0.2059	O2B, B2O
14	(Road, Person)	0.2078	O2B, B2O
15	(Fence, Traffic Sign)	0.2082	B2B
16	(Traffic Sign, Pole)	0.2092	B2B
17	(Fence, Person)	0.2150	O2B, B2O
18	(Pole, Vegetation)	0.2240	B2B
19	(Sidewalk, Pole)	0.2251	B2B
20	(Pole, Car)	0.2268	O2B, B2O

Impact of Poisoning Rate. Table 23 studies the effect of the poisoning rate (the percentage of training samples stamped with triggers) on attack performance. ASR increases monotonically as the poisoning rate grows. A similar trend is observed across all attack vectors, with B2O Attacks consistently reaching the highest ASRs. Notably, our attacks remain highly effective even at a low poisoning rate (0.05), whereas prior work typically relied on 0.1 to 0.2 to obtain practical backdoor performance [23, 40]. This highlights the efficiency of our poisoning strategy.

Comparison with Prior Work. We compare against three representative baselines: HBA [28], OFBA [40], and IBA [23]. In our studies, all three methods fall under the category of O2B Attacks. We re-implement these baselines under consistent hyperparameter settings to ensure fair comparison and evaluate them using ConvNeXt-T on BDD100K. The results in Table 24 show that our proposed attacks consistently out-

Table 22: Attack performance under different victim–target class configurations (fixed victim/target) for various attacks (complementary to Table 11).

(a) O2O: fixed victim (car), varying target (objects).

Victim	Target	ASR \uparrow	PBA \uparrow	CBA \uparrow
car	person	0.9352	0.6090	0.6265
	rider	0.9163	0.6102	0.6316
	truck	0.9307	0.6310	0.6369
	bus	0.9184	0.6223	0.6382
	train	0.9281	0.6366	0.6367
	motorcycle	0.9264	0.6006	0.6310
	bicycle	0.9303	0.5874	0.6227

(b) O2B: fixed victim (car), varying target (stuff).

Victim	Target	ASR \uparrow	PBA \uparrow	CBA \uparrow
car	road	0.9428	0.6283	0.6310
	sidewalk	0.9280	0.6214	0.6356
	building	0.9288	0.6197	0.6274
	wall	0.9058	0.6245	0.6195
	fence	0.9083	0.6228	0.6261
	pole	0.9187	0.6206	0.6280
	traffic light	0.9246	0.6116	0.6387
	traffic sign	0.9275	0.6069	0.6330
	vegetation	0.9427	0.6183	0.6147
	terrain	0.9154	0.6219	0.6281
	sky	0.9250	0.6374	0.6421

(c) O2B: fixed target (road), varying victim (objects).

Victim	Target	ASR \uparrow	PBA \uparrow	CBA \uparrow
person	road	0.7498	0.6422	0.6075
rider		0.4054	0.6516	0.6151
car		0.9428	0.6283	0.6310
truck		0.7264	0.6315	0.6147
bus		0.7850	0.6216	0.6163
train		0.0143	0.6530	0.6185
motorcycle		0.4051	0.6239	0.6125
bicycle		0.7968	0.6290	0.5942

perform prior approaches, confirming the effectiveness of our framework.

E Additional Experiments and Details on Defenses

STRIP [16] monitors prediction consistency when noise is added to model inputs, using entropy as a measure of this consistency. For clean inputs, perturbations produce random and varied predictions, yielding high entropy values. In contrast, backdoored inputs exhibit low entropy due to their consistently biased predictions toward the target class. To adapt STRIP for semantic segmentation models, we modify its approach from computing a single Shannon entropy value per input to generating an entropy map that captures per-pixel entropy across the segmentation mask. We then aggregate these pixel-wise scores into a unified metric for the entire image. This aggregated score serves as the decision criterion for identifying poisoned inputs. We evaluate STRIP’s detection performance using 250 clean and 250 poisoned samples, randomly sampled from the dataset. The threshold is deter-

Table 23: Results of various poisoning rates with ASR metrics.

Rate	0.05	0.1	0.2	0.3	0.5
O2O	0.8936	0.9212	0.9352	0.9346	0.9495
O2B	0.8794	0.9257	0.9428	0.9406	0.9423
B2O	0.9349	0.9621	0.9835	0.9877	0.9892
B2B	0.8996	0.915	0.9315	0.9267	0.9364
INS	0.8534	0.8891	0.9076	0.9143	0.9289
CON	0.8623	0.8956	0.9204	0.9267	0.9378

Table 24: Comparison between prior work and our attacks.

Method	HBA [28]	OFBA [40]	IBA [23]	Ours (O2O)	Ours (O2B)
ASR	0.1815	0.7859	0.8314	0.9352	0.9428
Method	Ours (B2O)	Ours (B2B)	Ours (Ins)	Ours (Con)	
ASR	0.9835	0.9315	0.9076	0.9204	

mined based on a target false positive rate (FPR): samples whose entropy lies below the FPR-th percentile of the clean entropy distribution are classified as poisoned samples. Figure 7 presents additional KDE plots of STRIP entropies. The results across different attacks indicate that the entropy distributions of clean and poisoned samples are highly overlapping and difficult to distinguish. This suggests that entropy-based detection is ineffective for backdoor attacks in semantic segmentation.

TeCo [30] operates on the principle that clean images exhibit consistent robustness patterns across different types of image corruptions. These corruptions include noise, blur, brightness changes, pixel-level perturbations, and image compression. For instance, an image robust to noise corruption typically demonstrates predictable robustness to blur corruption as well. Conversely, backdoor triggers exhibit inconsistent robustness profiles across different types of corruption. They may be resilient to certain corruptions while being highly sensitive to others, resulting in high variance in the severity required to disrupt the model’s prediction. To adapt TeCo for semantic segmentation models, we need to consider whether all labels on the prediction mask have changed. We compute the mIoU between the clean prediction mask and the corrupted prediction mask. A prediction is considered “broken” when the mIoU falls below a predefined threshold, indicating substantial degradation in segmentation quality under corruption. We adopt the 15 corruption types used in [30] and report the corresponding results, including *gaussian noise*, *shot noise*, *impulse noise*, *defocus blur*, *glass blur*, *motion blur*, *zoom blur*, *snow*, *frost*, *fog*, *brightness*, *contrast*, *elastic transform*, *pixelate*, and *jpeg compression*. We evaluate TeCo’s detection performance using 500 clean and 500 poisoned samples. Table 25 provides additional experimental results on defense methods. Figure 8 presents additional KDE plots of TeCo scores. The results across different attacks indicate that the score distributions of clean and poisoned samples are also highly overlapping. This suggests that TeCo is ineffective for

Table 25: Backdoor detection results under TeCo defense with additional evaluation metrics (complementary to Table 16).

Attack	1std				2std				3std			
	ACC	Recall	F1	AUC	ACC	Recall	F1	AUC	ACC	Recall	F1	AUC
HBA	0.568	0.2521	0.3494	0.5446	0.553	0.0652	0.1183	0.5169	0.540	0.0000	0.0000	0.5000
OFBA	0.583	0.2369	0.3433	0.5574	0.543	0.0630	0.1126	0.5074	0.540	0.0000	0.0000	0.5000
IBA	0.586	0.3112	0.4202	0.5765	0.529	0.0311	0.0599	0.5117	0.518	0.0000	0.0000	0.5000
O2O	0.528	0.1739	0.2532	0.5018	0.539	0.0478	0.0871	0.5026	0.540	0.0000	0.0000	0.5000
O2B	0.628	0.3826	0.4862	0.6098	0.560	0.0760	0.1373	0.5242	0.540	0.0000	0.0000	0.5000
B2O	0.558	0.1183	0.1754	0.4829	0.591	0.0377	0.0683	0.4965	0.603	0.0000	0.0000	0.5000
B2B	0.604	0.1445	0.1951	0.4885	0.655	0.0271	0.0496	0.4971	0.668	0.0000	0.0000	0.5000
INS	0.572	0.2134	0.3089	0.5312	0.548	0.0589	0.1067	0.5098	0.540	0.0000	0.0000	0.5000
CON	0.595	0.2687	0.3712	0.5523	0.556	0.0698	0.1245	0.5187	0.540	0.0000	0.0000	0.5000

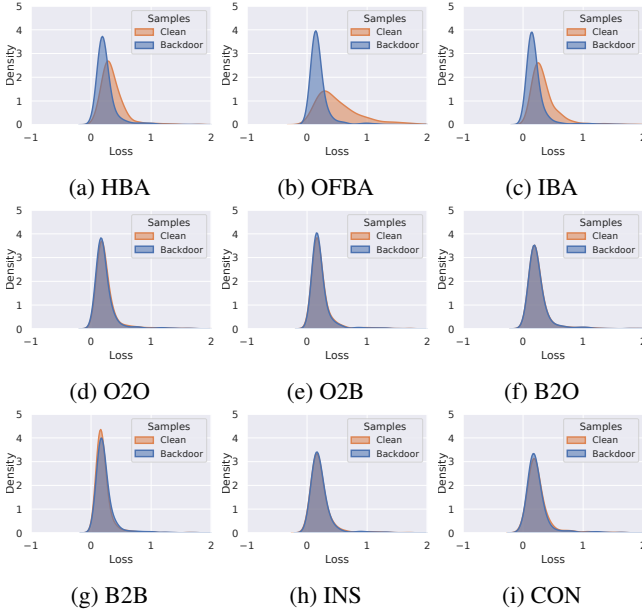


Figure 6: KDE plots of the losses of more attacks under ABL defense (complementary to Figure 5).

segmentation backdoor attacks.

Beatrix [38] analyzes subtle changes in a model’s internal activation patterns using Gramian information. The method operates on the principle that backdoor triggers induce statistically significant anomalies in the internal feature correlations of a model. It exploits this discrepancy by modelling the Gramian information of feature maps to distinguish between clean and poisoned samples. Adapting Beatrix to semantic segmentation models requires a class-wise sample grouping approach. In classification models, Beatrix leverages ground truth class labels to group input samples. It then calculates Gramian information within each group to identify poisoned samples. However, semantic segmentation models produce masks containing per-pixel class labels. This differs from single categorical predictions in classification tasks. To accommodate this structural difference, we adopt a straightforward adaptation strategy. For each ground truth segmentation mask, we identify the most dominant class, which is the class occupying the largest pixel area. We then use this dominant class as the grouping criterion for that sample. We evaluate Beat-

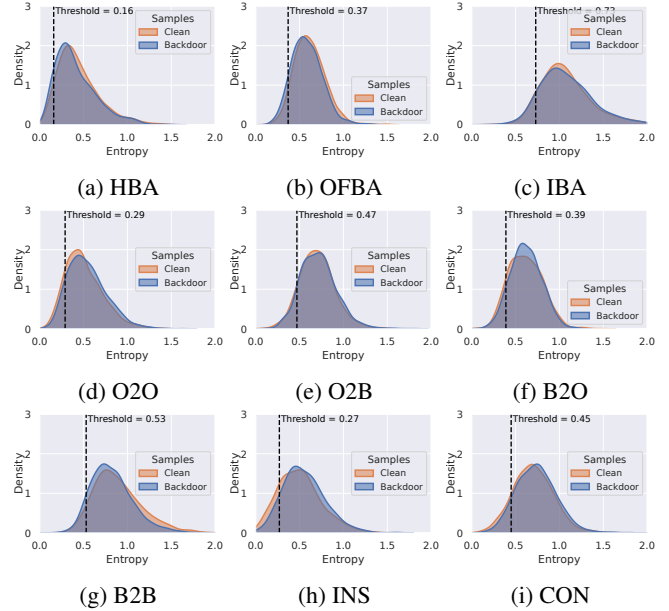


Figure 7: KDE plots of the entropy scores of more attacks under STRIP defense (complementary to Figure 5).

rix’s detection performance on 100 clean and 100 poisoned samples. The experimental results in Section 7 demonstrate that Beatrix is ineffective for segmentation backdoor attacks.

F Additional Discussion on Attacking Transformers

Prior work has shown that Transformer-based models are vulnerable to a range of privacy and security attacks [52, 59]. Table 18 reports backdoor attack results for ViT-B [11], DeiT-S [47], and Swin-T [33] on BDD100K. Across all settings, these transformers are comparably vulnerable to backdoor attacks on conventional segmentation models.

Performance of Swin-T. Swin-T and ConvNeXt-T both preserve strong local inductive biases and hierarchical multi-scale representations. ConvNeXt-T extracts local patterns through convolutions, while the Swin Transformer relies on windowed self-attention. In both cases, a localized trigger can be reliably captured in the early layers and passed through

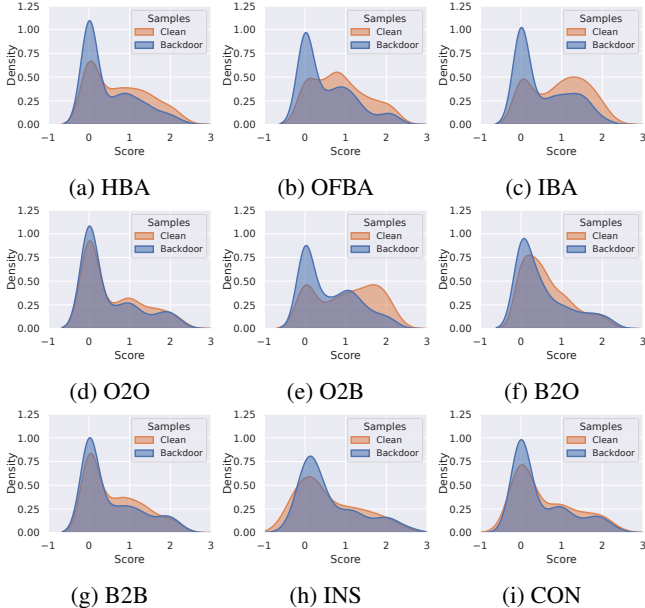


Figure 8: KDE plots of the detection scores of more attacks under TeCo defense (complementary to Figure 5).

the feature pyramid to the segmentation head. This locality and multi-scale feature extraction enable learning a stable trigger-to-mask manipulation, leading to comparable attack performance.

Performance of ViT-B and DeiT. ViT-B and DeiT tokenize images into patches, emphasizing global token interactions that can weaken the signal of small, localized triggers. The trigger may not consistently dominate attention across diverse scenes, making it harder for the model to learn a highly reliable backdoor. Nevertheless, their ASRs remain non-trivial, indicating that they are still clearly susceptible to backdoor attacks.

G Visualization

Figures 9 to 14 visualize our attacks on BDD100K, with one representative setting for each attack vector. In the O2O attack (Figure 9), the model maps the victim class *car* to the target class *person* once the trigger is present. In the O2B attack (Figure 10), the model maps *car* to the background class *road*. In the B2O attack (Figure 11), the model instead maps the background class *road* to the object class *car*, producing hallucinated object regions. In the B2B attack (Figure 12), the model maps *sidewalk* to *road* when triggers are injected into the victim region. In the INS attack (Figure 13), the trigger affects only the stamped object instance: the attacked *car* instance is flipped to *road*, while other *car* instances remain unchanged. In the CON attack (Figure 14), the backdoor behavior is conditioned on context: the model maps *car* to *road* only when the trigger appears on a red car. Overall,

these visualizations confirm the effectiveness of our attacks and illustrate how triggers can induce targeted yet context-dependent segmentation errors.

H Additional Related Work

Other Related Research. Some research explored backdoor triggers embedded within objects in images [3, 4, 9, 36], which relates to our coarse-grained attacks. These works primarily target object detection by manipulating bounding box predictions. In contrast, our attacks focus on semantic segmentation, manipulating individual pixel classifications to produce incorrect segmentation masks, requiring distinct trigger design strategies.

Some prior backdoor attacks [12, 44] share similarities with our fine-grained attacks, but key distinctions remain. In [12], they use a single condition (JPEG compression presence). However, our method requires composite conditions, which involve both a specific trigger pattern on an object and the object having particular attributes (i.e., a specific color). This enables more flexible, context-dependent attacks with enhanced stealthiness. In [44], they focused on model degradation rather than backdoor activation, whereas our method targets backdoor attacks through trigger and object associations.

I Discussion on Real-World Implementation

Our work identifies four coarse-grained attack vectors, defined by class-level semantic labels, and two fine-grained vectors, characterised by activation specificity. We discuss how these attacks could activate in a realistic autonomous-driving perception pipeline, where a backdoored segmentation model processes images captured by a front-facing camera.

We consider a practical adversary who can physically place a small trigger in the environment (e.g., near a roadway) but does not need to tamper with the victim vehicle. Once the trigger enters the camera’s field of view, the backdoored model may produce a manipulated segmentation mask while behaving normally on clean scenes. In practice, the geometric trigger can be printed (e.g., on paper or a sticker) and attached to common surfaces or objects with minimal effort.

For O2O, O2B and INS attacks, the trigger can be placed on the rear of a vehicle parked by the roadside, such that it appears in the captured scene when the victim car passes by. For B2O and B2B attacks, the trigger can be placed on planar background regions such as the road surface or sidewalk to induce false positives or background relabeling. For the CON attack, the trigger can be attached to a specific contextual object (e.g., the rear of a red car), causing activation only when the contextual condition is satisfied. As the victim vehicle approaches and captures the scene, the trigger becomes visible in one or more frames, activating the backdoor and causing the attacker-chosen manipulation.

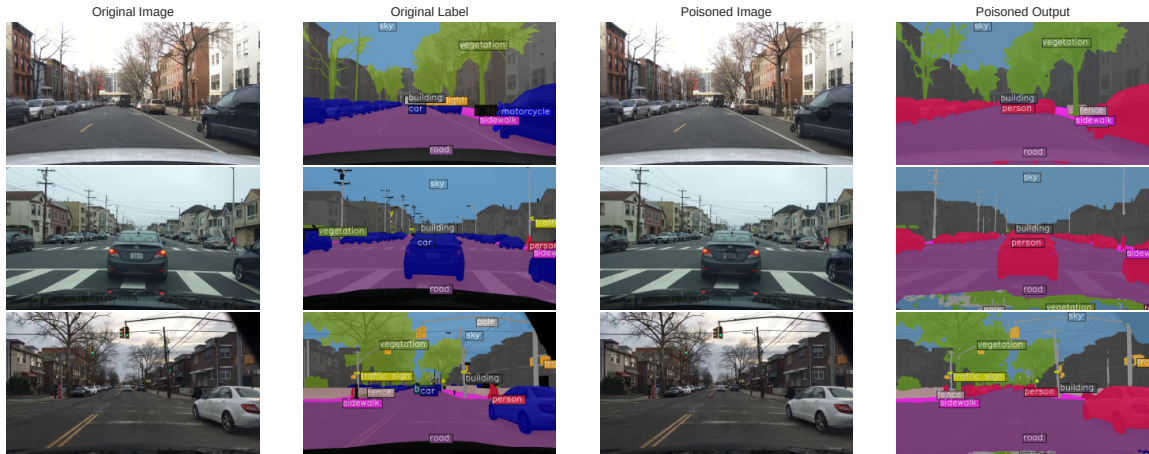


Figure 9: Visualization for O2O Attack.



Figure 10: Visualization for O2B Attack.

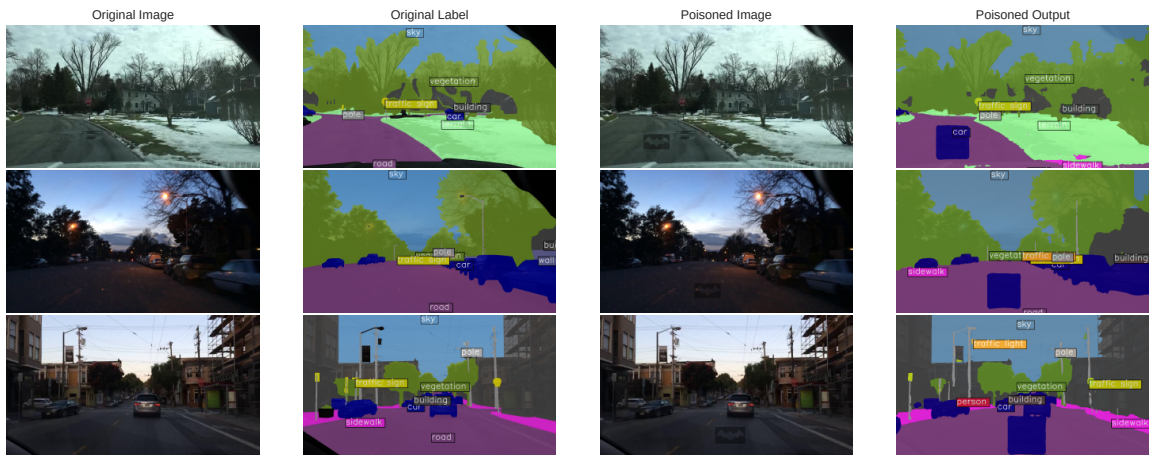


Figure 11: Visualization for B2O Attack.



Figure 12: Visualization for B2B Attack.

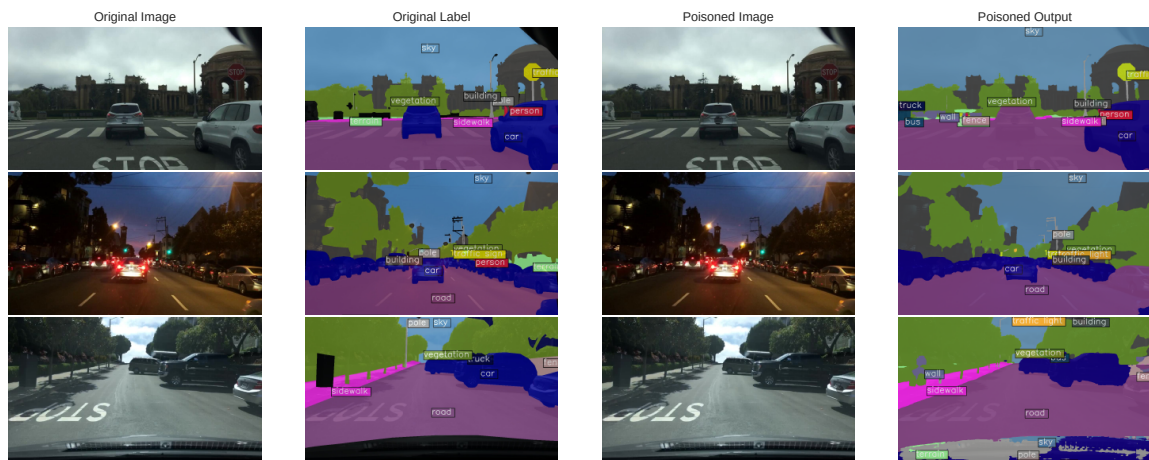


Figure 13: Visualization for Instance-Level Attack.



Figure 14: Visualization for Conditional Attack.